New Journal of Physics
The open access journal at the forefront of physics

Deutsche Physikalische Gesellschaft DPG IOP Institute of Physics

PAPER • OPEN ACCESS

Representation-free description of atom interferometers in time-dependent linear potentials

To cite this article: M Zimmermann *et al* 2019 *New J. Phys.* **21** 073031

New Journal of Physics
The open access journal at the forefront of physics

Deutsche Physikalische Gesellschaft DPG
IOP Institute of Physics

Published in partnership with: Deutsche Physikalische Gesellschaft and the Institute of Physics

OPEN ACCESS

RECEIVED
21 February 2019

REVISED
27 May 2019

ACCEPTED FOR PUBLICATION
2 July 2019

PUBLISHED
18 July 2019

PAPER

Representation-free description of atom interferometers in time-dependent linear potentials

M Zimmermann[1,6], **M A Efremov**[1], **W Zeller**[1], **W P Schleich**[1,2,3], **J P Davis**[4] and **F A Narducci**[5]

[1] Institut für Quantenphysik and Center for Integrated Quantum Science and Technology (IQST), Universität Ulm, D-89081 Ulm, Germany
[2] Hagler Institute for Advanced Study at Texas A&M University, Texas A&M AgriLife Research, Institute for Quantum Studies and Engineering (IQSE) and Department of Physics and Astronomy, Texas A&M University, College Station, TX 77843-4242, United States of America
[3] Institute of Quantum Technologies, German Aerospace Center (DLR), D-89069 Ulm, Germany
[4] AMPAC, North Wales, PA 19154, United States of America
[5] Department of Physics, Naval Postgraduate School, Monterey, CA 93943, United States of America
[6] Author to whom any correspondence should be addressed.

E-mail: matthias.zimmermann@uni-ulm.de **and** frank.narducci@nps.edu

Keywords: atom interferometry, precision measurements, representation-free formalism

Abstract

In this article we present a new representation-free formalism, which can significantly simplify the analysis of interferometers comprised of atoms moving in time-dependent linear potentials. We present a methodology for the construction of two pairs of time-dependent functions that, once determined, lead to two conditions for the closing of the interferometer, and determine the phase and the contrast of the resultant interference. Using this new formalism, we explore the dependency of the interferometer phase on the interferometer time T for different atom interferometers. By now, it is well established that light pulse atom interferometers of the type first demonstrated by Kasevich and Chu (1991 *Phys. Rev. Lett.* **67**, 181–4; 1992 *Appl. Phys.* B **54**, 321–32), henceforth referred to as Mach–Zehnder (MZ) atom interferometers, have a phase scaling as T^2. A few years ago, McDonald *et al* (2014 *Europhys. Lett.* **105**, 63001) have experimentally demonstrated a novel type of atom interferometer, referred to as the continuous-acceleration bloch (CAB) interferometer, where the phase reveals a mixed scaling which is governed by a combination of T^2 and T^3. Moreover, we have recently proposed a different type of atom interferometer (Zimmermann *et al* 2017 *Appl. Phys.* B **123**, 102), referred to as the T^3-interferometer, which has a *pure* T^3 scaling, as demonstrated theoretically. Finally, we conclude that the CAB interferometer can be shown to be a hybrid of the standard MZ interferometer and the T^3-interferometer.

1. Introduction

Atom interferometers [1–3] and in particular *light pulse* atom interferometers [4, 5] were first demonstrated in 1991. Since then different technologies and interferometer schemes have emerged, driven by the demand of high-sensitivity devices for precision measurements. In this article we compare three atom interferometers sensitive to linear accelerations by means of a novel formalism, which provides us with an intuitive picture for the scaling of their particular interferometric phase shift with respect to the interferometer time T[7].

1.1. Enhancing the sensitivity of atom interferometers

Because of their extreme interferometric sensitivity, atom interferometers have been used to precisely measure physical quantities such as the polarizability of alkali atoms [6–9], the 'magic wavelength' for potassium, rubidium and calcium [10–12], Planck's constant to the cesium mass ratio h/m_{Cs} [13], the fine structure

[7] We emphasize that in this article T always denotes the total interferometer time. This notation does in general not coincide with the traditional one, where T is used for the time between the first two laser pulses which is here labeled as T_1.

constant [14–18], and the Newtonian gravitational constant [19–22]. On a more applied side, there has been much activity in the development of interferometers as sensors of acceleration [23–43], rotation [44–47], gravity gradients [48–53], magnetic fields and magnetic field gradients [54–58], and dual accelerometer/gyroscopes [59–61]. Some of these works have been reviewed in [62, 63].

Despite the already demonstrated exquisite sensitivity of an atom interferometer, there are various ways to push it even further. The interferometer sensitivity usually depends on the mass of the particles in the interferometer [64], so using heavier atoms (e.g. rubidium or cesium instead of sodium) is one straightforward way for improvement. The sensitivity of the interferometer with respect to a constant acceleration or rotation also depends on the area enclosed by the interferometer [65–67]. This is due to the fact that light pulses not only create a coherent superposition of electronic states, but also transfer momentum. As a consequence, one finds the corresponding phase contribution to scale as the enclosed space-time area. Therefore, there have been several demonstrations of large-area interferometers by using composite and other more exotic pulses inducing a large momentum transfer [68–75].

For an interferometer in the conventional Mach–Zehnder (MZ) configuration, for instance, the enclosed area scales as T^2, where T is the total time of the interferometer. However, instead of increasing the effective momentum transferred by the pulses, there is an alternate way to improve the sensitivity of an interferometer by changing the interferometer scheme in order to achieve a different scaling of the phase with respect to T. McDonald *et al* [76] have demonstrated an interferometer measuring the gravitational acceleration with a combination of a T^2 and T^3 scaling, with the potential to achieve even higher-order scalings. Moreover, we have proposed an interferometer [77] with a *pure* T^3 scaling as acceleration sensor being sensitive to magnetic field gradients. Indeed, these three setups serve as motivation for this article: rederiving their scaling behavior by means of a representation-free description for interferometers in time- and state-dependent linear potentials.

Interestingly, also rotations and gravity gradients [78, 79] can lead to phase contributions, which are proportional to T^3. However, a discussion of these effects goes beyond the scope of this article.

1.2. An intuitive representation-free description of atom interferometers

In this article we develop a novel formalism based on the ideas and results presented in [80–82], valid for atoms moving in any time- and state-dependent linear potential. In order to determine the phase and contrast of an atom interferometer, the complete time evolution is usually split into *pieces* describing the time-evolution resulting from its basic building blocks: beam splitters, mirrors, and free propagation. This is generally the case within the path-integral approach [65], the ABCD formalism [83–85], and even in representation-free approaches based on operator methods [80, 86].

Within a representation-free formalism the resulting product of the corresponding unitary operators may lead to very complicated expressions, owing to the rise of nested commutators within the calculation as the Hamiltonian governing the evolution of the atoms does usually not commute with itself at different times. In contrast, our formalism involves time-dependent functions instead of operators. The action of the different building blocks directly enter into these functions, which immediately determine the *complete* time-evolution. Additionally, in our formalism momentum and phase changes imprinted by laser pulses and other external potentials are both described in a coherent way.

Essentially, we present a methodology to construct only two pairs of time-dependent functions $\{\mathbf{F}_\mathrm{u}(t),\ \omega_\mathrm{u}(t)\}$ and $\{\mathbf{F}_\mathrm{l}(t),\ \omega_\mathrm{l}(t)\}$ which we associate with the upper and lower branch of the interferometer, respectively. Two closing conditions are determined solely by the difference $\delta\mathbf{F}(t) \equiv \mathbf{F}_\mathrm{u}(t) - \mathbf{F}_\mathrm{l}(t)$ and lead to general expressions for the phase and contrast of the interferometer in terms of $\delta\mathbf{F}(t)$, $\bar{\mathbf{F}}(t) \equiv 1/2[\mathbf{F}_\mathrm{u}(t) + \mathbf{F}_\mathrm{l}(t)]$, and $\delta\omega(t) \equiv \omega_\mathrm{u}(t) - \omega_\mathrm{l}(t)$.

1.3. Outline

First, we use in section 2 a representation-free approach [80–82, 86, 87] and introduce beam splitters, mirrors, and free propagation in terms of unitary operators. We show how to combine these building blocks in order to obtain a general expression for the phase and contrast of the interference pattern. Next, in section 3 we present the details of our formalism describing atom interferometers exposed to time- and state-dependent linear potentials. Using the resulting schematic rules, we paint a new description of atom interferometers in section 4. Here we briefly describe the three types of atom interferometers mentioned before: (a) the MZ interferometer, (b) the T^3-interferometer, and (c) the continuous-acceleration bloch (CAB) interferometer, focusing on the different experimental realizations that lead to their particular T scaling. For each interferometer type, we use our formalism to calculate the T dependence of the phase of the interferometer, thereby showing the versatility and utility of our formalism. As a result of our analysis, we are also able to show that the CAB interferometer can be viewed as a hybrid between the MZ interferometer and the T^3-interferometer, which we discuss in section 5 before concluding in section 6.

In order to keep our article focused on the essential ideas, we present detailed calculations in four appendices. In appendix A we derive effective Hamiltonians corresponding to the upper and lower branch of the atom interferometer. Next, we determine in appendix B the dynamics induced by these Hamiltonians and analyse in appendix C the contrast and phase shift resulting from the interference of the two interferometer branches. Finally, we discuss in appendix D the phase shift of the CAB interferometer in detail.

2. Atom interferometers

The basic working principle of an atom interferometer is to coherently split the atomic wave packet into several components that probe the environment—especially the action of certain potentials such as the gravitational one—and to finally recombine the different components. After recombination the interference signal contains information about the interactions which have occurred within the interferometer.

In order to describe the atoms in our interferometer, we introduce an effective two-level system consisting of the two orthogonal states $|1\rangle$ and $|2\rangle$. Moreover, including the center-of-mass motion of the atoms in the state $|k\rangle$ $(k = 1, 2)$ described by $|\psi_k(t)\rangle$, we arrive at

$$|\Psi(t)\rangle = |\psi_1(t)\rangle|1\rangle + |\psi_2(t)\rangle|2\rangle \tag{1}$$

characterizing the entire atomic matter-wave at time t.

The three key steps in atom interferometry are (i) the initial preparation, (ii) the implementation of a certain interferometer sequence, and (iii) the final read-out. Typically, in step (i) only the state $|1\rangle$ is initially populated and the read-out in step (iii) also measures the population of this state. The interferometer sequences discussed in this article consist of two beam splitter pulses being separated by a period of free propagation, which may be interrupted by a certain number of mirror pulses.

2.1. Building blocks of atom interferometers

2.1.1. Free propagation

During free propagation the atom experiences no transitions between the two states $|1\rangle$ and $|2\rangle$. Therefore, the corresponding Hamiltonian

$$\hat{\mathcal{H}}_0 = \frac{\hat{\mathbf{p}}^2}{2m} \otimes \mathbb{1} + V_1(\hat{\mathbf{r}}, t) \otimes |1\rangle\langle 1| + V_2(\hat{\mathbf{r}}, t) \otimes |2\rangle\langle 2| \tag{2}$$

is diagonal in the $\{|1\rangle, |2\rangle\}$-basis with

$$\mathbb{1} = |1\rangle\langle 1| + |2\rangle\langle 2| \tag{3}$$

being the identity operator in the subspace spanned by these states. Here m denotes the atomic mass, and $\hat{\mathbf{r}}$ and $\hat{\mathbf{p}}$ are the position and momentum operators of the atomic center-of-mass motion, respectively.

Generally, the atom might probe two different potentials

$$V_k(\hat{\mathbf{r}}, t) = -\mathbf{F}_k(t)\hat{\mathbf{r}} + \hbar\omega_k(t), \tag{4}$$

which we both assume to be linear in position and are determined by the time-dependent functions $\mathbf{F}_k(t)$ and $\omega_k(t)$ corresponding to the state $|k\rangle$ $(k = 1, 2)$. The term proportional to $\mathbf{F}_k(t)$ may describe the interaction of the atom with a linear gravitational potential or the interaction of a magnetic dipole moment corresponding to the state $|k\rangle$ with a magnetic field having a constant gradient [54, 77]. In the latter case the potentials $V_k(\hat{\mathbf{r}}, t)$ become state-dependent if the mean values of the magnetic dipole moments corresponding to the two internal states differ. Specific examples of $\mathbf{F}_k(t)$ appear later in sections 3 and 4.

On the other hand, the term proportional to $\omega_k(t)$ in equation (4) may include the energy of an internal atomic state and additional time-dependent contributions due to, for instance, the interaction of magnetic-sensitive states with a homogeneous magnetic field. However, in the interaction picture with respect to $\omega_k(t)$ determined by the unitary operator

$$\hat{U}^{(\mathrm{I})}(t, t_\mathrm{i}) = \exp\left\{-\mathrm{i}\int_{t_\mathrm{i}}^{t} \mathrm{d}\tau\,[\omega_1(\tau)|1\rangle\langle 1| + \omega_2(\tau)|2\rangle\langle 2|]\right\}, \tag{5}$$

the contribution $\hbar\omega_k(t)$ to the potential $V_k(\hat{\mathbf{r}}, t)$, equation (4), can be absorbed in the time-evolution of the wave function during the free propagation. Here t_i denotes the initial time before applying the first beam splitter pulse. Hence, in this picture equation (2) for the Hamiltonian reads

$$\hat{\mathcal{H}} = \frac{\hat{\mathbf{p}}^2}{2m} \otimes \mathbb{1} - \mathbf{F}_1(t)\hat{\mathbf{r}} \otimes |1\rangle\langle 1| - \mathbf{F}_2(t)\hat{\mathbf{r}} \otimes |2\rangle\langle 2| \tag{6}$$

leading to the evolution operator

$$\hat{\mathcal{E}}(t_b,\, t_a) = \begin{pmatrix} \hat{E}_{22}(t_b,\, t_a) & 0 \\ 0 & \hat{E}_{11}(t_b,\, t_a) \end{pmatrix} \tag{7}$$

between the times t_a and t_b. Here we have introduced the time evolution operator $\hat{E}_{kk}(t_b,\, t_a)$ corresponding to the Hamiltonian

$$\hat{H}_k = \frac{\hat{\mathbf{p}}^2}{2m} - \mathbf{F}_k(t)\hat{\mathbf{r}} \tag{8}$$

with $k = 1, 2$.

2.1.2. Beam-splitter and mirror pulses

In this section we describe perfect beam-splitter and mirror pulses for an atom interferometer. As it is often done [80], we assume that these pulses are so short that the atomic center-of-mass motion during the pulses may be neglected. As a result, these pulses act instantaneously at a given time t_j. Indeed, the interaction of an atom with a near resonant electromagnetic field may fulfill this requirement and thus offers an experimental realization for beam splitters ($\pi/2$-pulse) and mirrors (π-pulse). However, we note that the consequences of a finite pulse duration are discussed in [88, 89].

In order to describe the atom-light interaction we include the effects of a possible momentum transfer $\hbar\mathbf{k}$ and a laser phase $\phi(t_j)$. Using the effective wave vector $\mathbf{k}$ and the effective phase

$$\Phi(t_j) = \phi(t_j) - \omega_{\mathrm{L}} t_j + \int_{t_{\mathrm{i}}}^{t_j} \mathrm{d}\tau\, [\omega_2(\tau) - \omega_1(\tau)] \tag{9}$$

depending on the laser frequency ω_{L}, we obtain [80, 88, 90, 91] the unitary beam splitter operator

$$\hat{\mathcal{B}}(t_j) = \frac{1}{\sqrt{2}} \begin{pmatrix} 1 & \hat{L}_+(t_j) \\ \hat{L}_-(t_j) & 1 \end{pmatrix} \tag{10}$$

in the frame defined by equation (5), assuming $\omega_2(t_j) > \omega_1(t_j)$. The operator $\hat{\mathcal{B}}(t_j)$ creates an equally weighted superposition of the two states $|1\rangle$ and $|2\rangle$ and is determined by the unitary operator

$$\hat{L}_\pm(t_j) = -\mathrm{i}\exp\{\pm\mathrm{i}[\mathbf{k}\hat{\mathbf{r}} + \Phi(t_j)]\}. \tag{11}$$

Here the prefactor $1/\sqrt{2}$ in equation (10) ensures the unitarity of the operator $\hat{\mathcal{B}}(t_j)$.

A perfect mirror instead should create a perfect inversion of the populations of the states $|1\rangle$ and $|2\rangle$. This case is described by the unitary operator

$$\hat{\mathcal{M}}(t_j) = \begin{pmatrix} 0 & \hat{L}_+(t_j) \\ \hat{L}_-(t_j) & 0 \end{pmatrix} \tag{12}$$

with $\hat{L}_\pm(t_j)$ being defined by equation (11). It is important to emphasize that these ideal beam-splitter and mirror pulses imprint additional phases and lead to displacements in momentum of $\pm\hbar\mathbf{k}$ without distortion of the center-of-mass wave packet.

2.2. Interferometer sequence

We have now all the ingredients at hand to construct the atom interferometers discussed in detail in section 4. Indeed, each interferometer consists of a period of free evolution (t_{i}, t_1), an opening beam splitter pulse applied at time t_1, followed by a number of $n - 1$ periods $(t_1, t_2), (t_2, t_3), \ldots, (t_{n-1}, t_n)$ of free evolution, being separated by $n - 2$ mirror pulses applied at times $t_j\,(j = 2, \ldots, n - 1)$, and a closing beam splitter pulse applied at time t_n, followed by a free evolution period (t_n, t_{f}), as depicted in figure 1.

In order to describe such an interferometer sequence with instantaneous laser pulses, we use the building blocks presented by equations (7), (10), and (12), and obtain the total evolution operator

$$\hat{\mathcal{U}}(t_{\mathrm{f}},\, t_{\mathrm{i}}) = \hat{\mathcal{E}}(t_{\mathrm{f}},\, t_n)\hat{\mathcal{B}}(t_n)\hat{\mathcal{E}}(t_n,\, t_{n-1})\hat{\mathcal{M}}(t_{n-1}) \ldots \hat{\mathcal{E}}(t_3,\, t_2)\hat{\mathcal{M}}(t_2)\hat{\mathcal{E}}(t_2,\, t_1)\hat{\mathcal{B}}(t_1)\hat{\mathcal{E}}(t_1,\, t_{\mathrm{i}}) \tag{13}$$

of this interferometer with the initial time $t_{\mathrm{i}} < t_1$ and the final time $t_{\mathrm{f}} > t_n$.

Now we use the facts that the free evolution operator $\hat{\mathcal{E}}$, equation (7), is diagonal and the operator $\hat{\mathcal{M}}$, equation (12), is anti-diagonal in the $\{|1\rangle,\, |2\rangle\}$-basis. In this case, the operator

$$\hat{U}_{11} = \langle 1|\hat{\mathcal{U}}(t_{\mathrm{f}},\, t_{\mathrm{i}})|1\rangle \equiv \frac{1}{2}[\hat{U}_{\mathrm{u}} + \hat{U}_{\mathrm{l}}], \tag{14}$$

describing the time evolution of the atom being prepared in $|1\rangle$ and detected in $|1\rangle$, is determined by the sum of the evolution operators

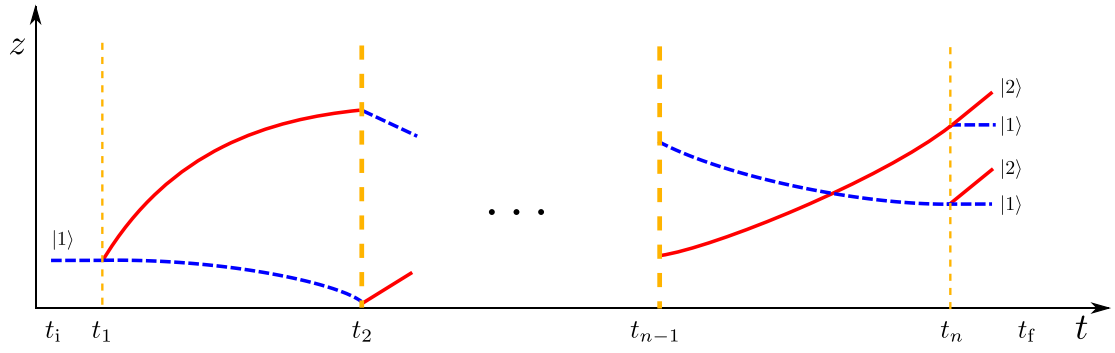

Figure 1. A one-dimensional sketch of a space-time diagram of a general two-branch interferometer for a two-level atom having the states $|1\rangle$ (dashed blue line) and $|2\rangle$ (solid red line), and being exposed to a time- and state-dependent linear potential. The atom interacts with two beam splitter pulses at times t_1 and t_n and $n-2$ mirror pulses at times t_j ($j = 2, \ldots, n-1$).

$$\hat{U}_\mathrm{u} = 2\hat{E}_{11}(t_\mathrm{f}, t_n)\hat{B}_{12}(t_n)\hat{E}_{22}(t_n, t_{n-1})\hat{M}_{21}(t_{n-1}) \ldots \hat{E}_{11}(t_3, t_2)\hat{M}_{12}(t_2)\hat{E}_{22}(t_2, t_1)\hat{B}_{21}(t_1)\hat{E}_{11}(t_1, t_\mathrm{i}) \tag{15}$$

for the upper branch and

$$\hat{U}_\mathrm{l} = 2\hat{E}_{11}(t_\mathrm{f}, t_n)\hat{B}_{11}(t_n)\hat{E}_{11}(t_n, t_{n-1})\hat{M}_{12}(t_{n-1}) \ldots \hat{E}_{22}(t_3, t_2)\hat{M}_{21}(t_2)\hat{E}_{11}(t_2, t_1)\hat{B}_{11}(t_1)\hat{E}_{11}(t_1, t_\mathrm{i}) \tag{16}$$

for the lower branch of the interferometer with an *even* number of pulses. Here we have introduced the notation

$$\hat{B}_{ik}(t_j) \equiv \langle i|\hat{\mathcal{B}}(t_j)|k\rangle \tag{17}$$

and

$$\hat{M}_{ik}(t_j) \equiv \langle i|\hat{\mathcal{M}}(t_j)|k\rangle. \tag{18}$$

With equations (10) and (12) we recast equations (15) and (16) in terms of the operator $\hat{L}_\pm(t_j)$ as

$$\hat{U}_\mathrm{u} = \hat{E}_{11}(t_\mathrm{f}, t_n)\hat{L}_-(t_n)\hat{E}_{22}(t_n, t_{n-1})\hat{L}_+(t_{n-1}) \ldots \hat{E}_{11}(t_3, t_2)\hat{L}_-(t_2)\hat{E}_{22}(t_2, t_1)\hat{L}_+(t_1)\hat{E}_{11}(t_1, t_\mathrm{i}) \tag{19}$$

and

$$\hat{U}_\mathrm{l} = \hat{E}_{11}(t_\mathrm{f}, t_{n-1})\hat{L}_-(t_{n-1}) \ldots \hat{E}_{22}(t_3, t_2)\hat{L}_+(t_2)\hat{E}_{11}(t_2, t_\mathrm{i}), \tag{20}$$

accordingly.

Similarly, for an *odd* number of pulses we obtain instead

$$\hat{U}_\mathrm{u} = \hat{E}_{11}(t_\mathrm{f}, t_{n-1})\hat{L}_-(t_{n-1}) \ldots \hat{E}_{11}(t_3, t_2)\hat{L}_-(t_2)\hat{E}_{22}(t_2, t_1)\hat{L}_+(t_1)\hat{E}_{11}(t_1, t_\mathrm{i}) \tag{21}$$

and

$$\hat{U}_\mathrm{l} = \hat{E}_{11}(t_\mathrm{f}, t_n)\hat{L}_-(t_n)\hat{E}_{22}(t_n, t_{n-1})\hat{L}_+(t_{n-1}) \ldots \hat{E}_{22}(t_3, t_2)\hat{L}_+(t_2)\hat{E}_{11}(t_2, t_\mathrm{i}). \tag{22}$$

It is important to recall that the operators $\hat{U}_\mathrm{u}$ and $\hat{U}_\mathrm{l}$ are unitary by construction and describe the time evolution from t_i to t_f for the upper and lower branch of the interferometer, respectively.

Next, we relate these operators $\hat{U}_\mathrm{u}$ and $\hat{U}_\mathrm{l}$ to the observables such as the contrast and phase of the interferometer. Assuming an atom being prepared in the state $|1\rangle$ corresponding to the initial state

$$|\Psi(t_\mathrm{i})\rangle = |\psi_\mathrm{i}\rangle|1\rangle, \tag{23}$$

where $|\psi_\mathrm{i}\rangle$ describes the initial state of the center-of-mass motion, the probability $P_{11}(t_\mathrm{f})$ to observe atoms in the state $|1\rangle$ after the closing beam splitter pulse (at $t = t_n$), as shown in figure 1, is thus given by

$$P_{11}(t_\mathrm{f}) = \langle\Psi(t_\mathrm{f})|1\rangle\langle 1|\Psi(t_\mathrm{f})\rangle = \langle\Psi(t_\mathrm{i})|\hat{\mathcal{U}}^\dagger(t_\mathrm{f}, t_\mathrm{i})|1\rangle\langle 1|\hat{\mathcal{U}}(t_\mathrm{f}, t_\mathrm{i})|\Psi(t_\mathrm{i})\rangle. \tag{24}$$

Applying equation (14), we arrive at

$$P_{11}(t_\mathrm{f}) = \langle\psi_\mathrm{i}|\hat{U}_{11}^\dagger\hat{U}_{11}|\psi_\mathrm{i}\rangle = \frac{1}{2}[1 + C\cos(\delta\phi)], \tag{25}$$

where the contrast C and phase $\delta\phi$ of the interferometer are the modulus and argument of the matrix element

$$\langle\psi_\mathrm{i}|\hat{U}_\mathrm{l}^\dagger\hat{U}_\mathrm{u}|\psi_\mathrm{i}\rangle \equiv Ce^{\mathrm{i}\delta\phi} \tag{26}$$

of the operator product $\hat{U}_\mathrm{l}^\dagger\hat{U}_\mathrm{u}$ determined by the initial state $|\psi_\mathrm{i}\rangle$ of the center-of-mass motion. In the case that the atom is prepared in state $|1\rangle$, but measured in state $|2\rangle$, the probability reads

$$P_{21}(t_f) = \frac{1}{2}[1 - C\cos(\delta\phi)]. \tag{27}$$

3. An intuitive picture of the interferometer

3.1. Interferometer contrast and phase

In the preceding section we have shown that the contrast C and the interferometer phase $\delta\phi$ are both determined by the matrix element $\langle\psi_i|\hat{U}_l^\dagger \hat{U}_u|\psi_i\rangle$, equation (26). The operator $\hat{U}_b$, equations (19)–(22), describes the time evolution along the upper (b = u) and lower (b = l) branch of the interferometer. As shown in appendix A, this operator can be associated with the effective Hamiltonian

$$\hat{H}_b(t) = \frac{\hat{\mathbf{p}}^2}{2m} - \mathbf{F}_b(t)\hat{\mathbf{r}} + \hbar\omega_b(t) \tag{28}$$

determined by the time-dependent functions $\omega_b(t)$ and $\mathbf{F}_b(t)$, accordingly. In appendix B we obtain the time-evolution operator $\hat{U}_b(t,\ t_i)$ in terms of these functions, and find in appendix C a general expression for the operator product

$$\hat{U}_l^\dagger \hat{U}_u = \exp[i\Delta\phi(t_f)]\hat{D}\left[\delta\mathbf{r}(t_f) - \frac{\delta\mathbf{p}(t_f)}{m}(t_f - t_i),\ \delta\mathbf{p}(t_f)\right]. \tag{29}$$

Here $\Delta\phi(t_f)$ is a phase factor and

$$\hat{D}[\mathbf{R},\ \mathbf{P}] = \exp\left[-\frac{i}{\hbar}(\mathbf{R}\hat{\mathbf{p}} - \mathbf{P}\hat{\mathbf{r}})\right] \tag{30}$$

is the displacement operator with arguments $\mathbf{P}$ and $\mathbf{R}$ being determined in equation (29) by the time-dependent vectors

$$\delta\mathbf{p}(t) = \int_{t_i}^{t} d\tau\ \delta\mathbf{F}(\tau) \tag{31}$$

and

$$\delta\mathbf{r}(t) = \frac{1}{m}\int_{t_i}^{t} d\tau_1 \int_{t_i}^{\tau_1} d\tau_2\ \delta\mathbf{F}(\tau_2) \tag{32}$$

with

$$\delta\mathbf{F}(t) \equiv \mathbf{F}_u(t) - \mathbf{F}_l(t). \tag{33}$$

Indeed, the vectors $\delta\mathbf{p}(t)$ and $\delta\mathbf{r}(t)$ correspond to the relative displacements in momentum and position between the two classical trajectories associated with the two branches of the interferometer, respectively [82].

In order to maximize the interferometer contrast

$$C = \left|\langle\psi_i|\ \hat{D}\left[\delta\mathbf{r}(t_f) - \frac{\delta\mathbf{p}(t_f)}{m}(t_f - t_i),\ \delta\mathbf{p}(t_f)\right]|\psi_i\rangle\right| \tag{34}$$

independently of the initial state $|\psi_i\rangle$, we require that the operator $\hat{D}$ in equation (34) is the identity operator, which leads us to the closing conditions of the interferometer, that is

$$\delta\mathbf{p}(t_f) = \int_{t_i}^{t_f} d\tau\ \delta\mathbf{F}(\tau) = 0 \tag{35}$$

and

$$\delta\mathbf{r}(t_f) = \frac{1}{m}\int_{t_i}^{t_f} d\tau_1 \int_{t_i}^{\tau_1} d\tau_2\ \delta\mathbf{F}(\tau_2) = 0, \tag{36}$$

or the relative displacements in momentum and position between the two branches should vanish at the final time t_f. In this case we speak of a *closed* interferometer.

Consequently, the interferometer phase

$$\delta\phi = \Delta\phi(t_{\rm f}) = \delta\phi_0 + \delta\phi_1 \tag{37}$$

is a sum of two phases

$$\delta\phi_0 \equiv -\int_{t_{\rm i}}^{t_{\rm f}} {\rm d}\tau\ \delta\omega(\tau) \tag{38}$$

and

$$\delta\phi_1 \equiv \frac{1}{\hbar}\int_{t_{\rm i}}^{t_{\rm f}} {\rm d}\tau\ \bar{\rm F}(\tau)\delta{\bf r}(\tau) \tag{39}$$

with

$$\delta\omega(t) \equiv \omega_{\rm u}(t) - \omega_{\rm l}(t) \tag{40}$$

and

$$\bar{\rm F}(t) \equiv \frac{1}{2}[{\rm F}_{\rm u}(t) + {\rm F}_{\rm l}(t)]. \tag{41}$$

We emphasize that the interferometer phase $\delta\phi$ is independent of the initial state $|\psi_{\rm i}\rangle$ for a *closed* interferometer. Moreover, for $\bar{\rm F}$ being time-independent, the phase contribution $\delta\phi_1$, equation (39), is proportional to the *enclosed area* between the upper and lower branch of the interferometer in the space-time diagram, shown in figure 1. In the case that the two interferometer branches cross in space, it is the signed area which is relevant. Needless to say that the general result derived in appendix C agrees with the considerations presented in [81, 82] which are valid for both Raman and Bragg diffraction. In the special case of a *closed* interferometer, equation (37) coincides with the result obtained within the semi-classical description [67].

3.2. Schematic rules

Now we are in the position to summarize our scheme in order to obtain the contrast and phase of the general interferometer presented in figure 1.

The key ingredient of our method is the construction of only two pairs of time-dependent functions $\{{\rm F}_{\rm u}(t),\ \omega_{\rm u}(t)\}$ and $\{{\rm F}_{\rm l}(t),\ \omega_{\rm l}(t)\}$ corresponding to the upper and lower branch of the atom interferometer, accordingly, as depicted in figure 2. Here a dashed blue line indicates the state $|1\rangle$ while a solid red line corresponds to the state $|2\rangle$.

Since the initial state is assumed to be prepared in the state $|1\rangle$, equation (23), both branches start from the dashed line. The procedure to obtain the functions $\omega_{\rm b}(t)$ and ${\bf F}_{\rm b}(t)$ (b = u, l), as well as the contrast and phase of the interferometer consists of four steps.

Step 1: Each function $\omega_{\rm b}(t)$ is the sum of all contributions arising from position-independent potentials and consists of summands[8] having the form $-\Phi_-\ (t)\delta(t - t_j)$ at the transition $|1\rangle \to |2\rangle$ (change from dashed to solid line) or $\Phi_+\ (t)\delta(t - t_j)$ at the transition $|2\rangle \to |1\rangle$ (change from solid to dashed line), where

$$\Phi_\mp(t_j) \equiv \Phi(t_j) \mp \frac{\pi}{2}, \tag{42}$$

and $\Phi(t_j)$ is defined by equation (9). The difference $\delta\omega(t)$, equation (40), of the functions $\omega_{\rm b}(t)$ for the upper and lower branch determines the contribution $\delta\phi_0$, equation (38), to the interferometer phase.

Step 2: Each function ${\bf F}_{\rm b}(t)$ is the sum of all contributions (see footnote 6) presented in figure 2 originating from (i) the free evolution between pulses applied at the times $t = t_j$ and $t = t_{j+1}$, that is ${\bf F}_1(t)\,\Pi(t|t_j,\ t_{j+1})$ (dashed blue line) and ${\bf F}_2(t)\,\Pi(t|t_j,\ t_{j+1})$ (solid red line) for an atom in the state $|1\rangle$ or $|2\rangle$, respectively, and (ii) the momentum kick $\hbar{\bf k}\delta(t - t_j)$ at the transition $|1\rangle \to |2\rangle$ (change from dashed to solid line), or $-\hbar{\bf k}\delta(t - t_j)$ at the transition $|2\rangle \to |1\rangle$ (change from solid to dashed line).

Step 3: Obtain the difference $\delta{\bf F}(t)$ of the functions ${\bf F}_{\rm b}(t)$ defined by equation (33), as well as the functions $\delta{\bf p}(t)$, equation (31), and $\delta{\bf r}(t)$, equation (32), and check the two closing conditions (35) and (36).

Step 4(a): If the interferometer is closed, the contrast $C = 1$. Find the function $\bar{\rm F}(t)$ defined by equation (41), which determines together with $\delta{\bf r}(t)$ the contribution $\delta\phi_1$, equation (39). The interferometer phase $\delta\phi$, equation (37), is the sum of $\delta\phi_0$ and $\delta\phi_1$.

[8] Here $\delta(t)$ denotes the Dirac delta function and $\Pi(t|a,\ b)$ is the rectangular function of unit height on the interval (a, b) as defined in equation (43).

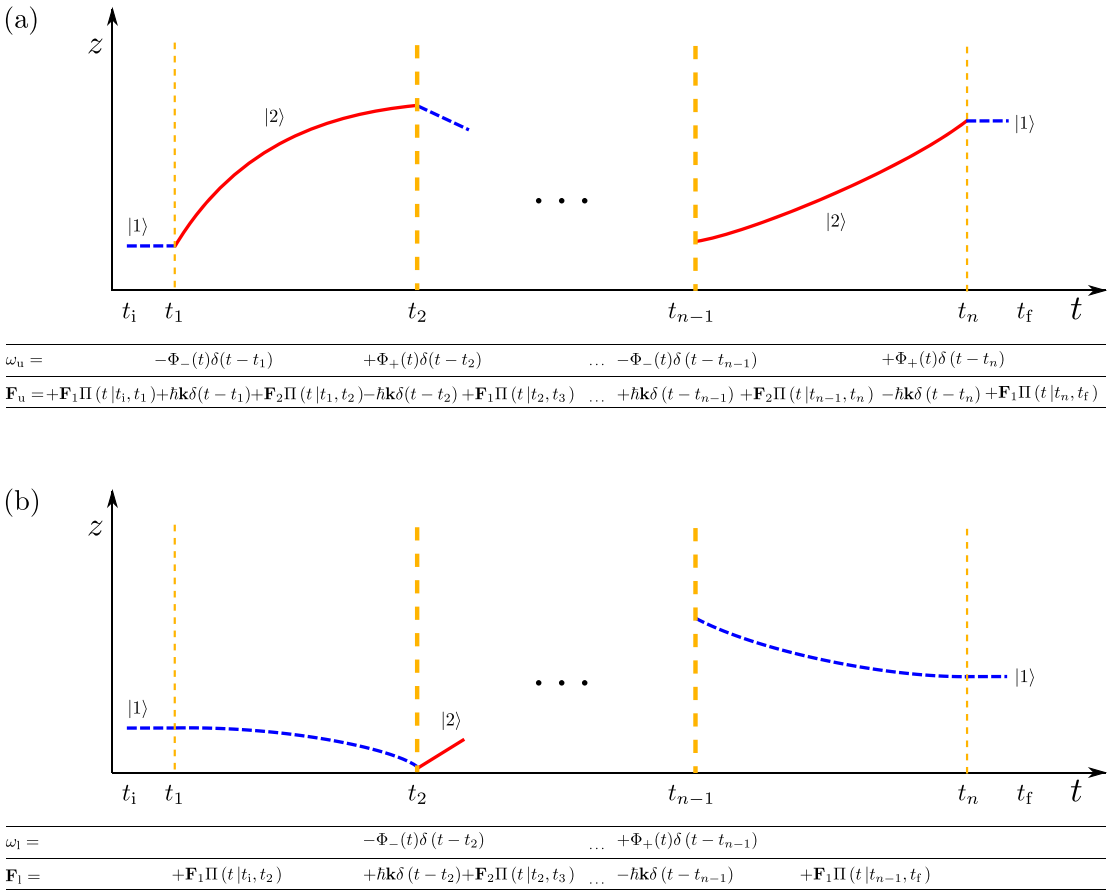

Figure 2. Upper (a) and lower (b) branch of the space-time diagram for the interferometer presented in figure 1. Below each diagram we show a pair of the corresponding time-dependent functions $\omega_b(t)$ and $\mathbf{F}_b(t)$ (b = u, l). Each function $\omega_b(t)$ is a sum of all contributions arising from position-independent potentials and contains (see footnote 6) the scalar terms $\mp\Phi_\mp(t)\delta(t-t_j)$, as defined by equations (9) and (42). Moreover, each function $\mathbf{F}_b(t)$ is a sum of (i) contributions $\mathbf{F}_k\Pi(t|t_j, t_{j+1})$ describing the free evolution of the atom in the state $|k\rangle$ (for $k = 1, 2$), where $|1\rangle$ and $|2\rangle$ correspond to a dashed blue and solid red line, and (ii) the momentum kicks $+\hbar\mathbf{k}\delta(t-t_j)$ and $-\hbar\mathbf{k}\delta(t-t_j)$ for the transition $|1\rangle \to |2\rangle$ and $|2\rangle \to |1\rangle$, respectively. Here $j = 1, \ldots n$, where n is the number of pulses.

Step 4(b): If the interferometer is not closed, then the contrast C is given by equation (34) and depends on $\delta\mathbf{r}(t_f)$, $\delta\mathbf{p}(t_f)$, as well as the initial state $|\psi_i\rangle$. Its phase $\delta\phi$ is derived in appendix C.1.

4. A comparison of three atom interferometers

In this section we apply our formalism introduced in section 3 to the MZ interferometer [4, 5, 54, 65, 80, 84, 88, 92], the T^3-interferometer [77], and the CAB interferometer [76]. We extend the analysis of these interferometers discussed briefly in [77]. As a result of our formalism, we present a simple explanation of the different scalings of the interferometer phase with respect to the total interferometer time T. In particular, we show that the CAB interferometer is a combination of the MZ and the T^3-interferometer. Moreover, we discuss the different experimental techniques used to imprint forces, namely Raman transitions, magnetic field gradients, Bragg transitions, and Bloch oscillations.

In order to obtain a coherent description of these interferometers, we introduce the following family of functions vanishing outside the interval (a, b) with $a < b$ and $c \equiv (a + b)/2$, which are based on the Dirac delta function $\delta(t)$.

- The rectangular function

$$\Pi(t|a, b) \equiv \int_{-\infty}^{t} \mathrm{d}\tau[\delta(\tau - a) - \delta(\tau - b)] \tag{43}$$

of unit height.

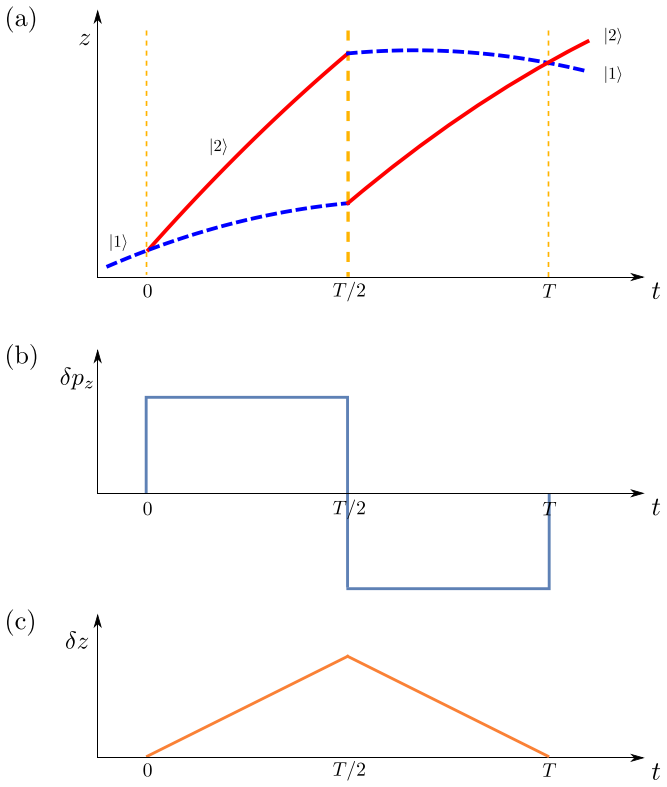

Figure 3. (a) Space-time diagram of a standard Mach–Zehnder type interferometer in a linear potential for an atom having the two internal states $|1\rangle$ and $|2\rangle$. The atom interacts with two short laser $\pi/2$-pulses (at $t = 0$ and $t = T$) and a π-pulse (at $t = T/2$), where T is the total interferometer time. During each pulse the atom absorbs (emits) the momentum $\hbar\mathbf{k}$ in combination with the transition $|1\rangle \rightarrow |2\rangle$ ($|2\rangle \rightarrow |1\rangle$). The z-component of the relative displacements in (b) momentum $\delta\mathbf{p}(t)$, equation (55), and (c) position $\delta\mathbf{r}(t)$, equation (56), as a function of time t.

- The triangular function

$$\Lambda(t|a, b) \equiv \int_{-\infty}^{t} \mathrm{d}\tau\,[\Pi(\tau|a, c) - \Pi(\tau|c, b)] \tag{44}$$

  with the height $(b - a)/2$.

- The piece-wise quadratic function

$$\Omega(t|a, b) \equiv \int_{-\infty}^{t} \mathrm{d}\tau\,[\Lambda(\tau|a, c) - \Lambda(\tau|c, b)] \tag{45}$$

  with the height $(b - a)^2/16$.

4.1. MZ interferometer

4.1.1. Description

We briefly review the physics underlying the basic MZ atom interferometer, emphasizing the points salient to this article. In particular, we discuss the origin of the scaling of the interferometer phase with T^2.

A standard MZ type atom interferometer is depicted in figure 3(a). For this interferometer type we focus on the case of driving Raman transitions between two ground electronic states, labeled $|1\rangle$ and $|2\rangle$. Atoms entering the interferometer have usually been prepared in the state $|1\rangle$. The atoms are subject to a beam-splitter pulse applied at time $t_1 = 0$ which creates a coherent superposition of states $|1\rangle$, shown by a blue dashed curve in figure 3(a), and $|2\rangle$, depicted by a red solid curve. Subsequently, the atoms evolve in the dark for a time $T/2$. Then they experience a mirror pulse at $t_2 = T/2$, which causes the states to 'flip', that is $|1\rangle \rightarrow |2\rangle$ and $|2\rangle \rightarrow |1\rangle$. The atoms evolve again in the dark for another time $T/2$. Finally, the two arms of the interferometer are recombined with a final beam splitter pulse at $t_3 = T$.

In the case of the MZ interferometer both states $|1\rangle$ and $|2\rangle$ are exposed to the same linear time-independent potential leading to

$$\mathbf{F}_1(t) = \mathbf{F}_2(t) \equiv \mathbf{F}_0 \tag{46}$$

for the functions $\mathbf{F}_{1,2}(t)$ in equations (4), (6), and (8).

This is the case for atoms being exposed to (i) the gravitational field [4, 5] with the constant gravitational acceleration $\mathbf{g}$, where $\mathbf{F}_0 = m\mathbf{g}$, and (ii) the magnetic field

$$\mathbf{B}(\mathbf{r}) = (B_0 + z\nabla_z B_z)\mathbf{e}_z \tag{47}$$

with constant gradient $\nabla_z B_z$ and the unit vector $\mathbf{e}_z$ in the z-direction[9]. The latter case leads to $\mathbf{F}_0 = \mu_z \nabla_z B_z \mathbf{e}_z$, when the atom has the *same* z-component of the mean value of the magnetic dipole moment $\mu_z = \mu_{1z} = \mu_{2z}$ with $\boldsymbol{\mu}_k \equiv \langle k|\hat{\boldsymbol{\mu}}|k\rangle$ $(k = 1, 2)$ for the states $|1\rangle$ and $|2\rangle$, as presented in [54].

As shown below, the relative displacement in momentum $\delta\mathbf{p}(t)$ between the two branches of the interferometer is piece-wise constant, figure 3(b), whereas the relative displacement in position $\delta\mathbf{r}(t)$ is piece-wise linear in t, figure 3(c), leading to an interferometer phase scaling as T^2.

4.1.2. Analysis of the MZ interferometer

According to Step 1 of our procedure (section 3.2), as well as to figures 2 and 3(a), we arrive at

$$\omega_{\mathrm{u}}(t) = -\Phi_-(0)\delta(t) + \Phi_+\left(\frac{T}{2}\right)\delta\left(t - \frac{T}{2}\right) \tag{48}$$

for the upper branch together with

$$\omega_{\mathrm{l}}(t) = -\Phi_-\left(\frac{T}{2}\right)\delta\left(t - \frac{T}{2}\right) + \Phi_+(T)\delta(t - T) \tag{49}$$

for the lower branch of the MZ interferometer determining the difference

$$\delta\omega(t) = -\Phi_-(0)\delta(t) + \left[\Phi_+\left(\frac{T}{2}\right) + \Phi_-\left(\frac{T}{2}\right)\right]\delta\left(t - \frac{T}{2}\right) - \Phi_+(T)\delta(t - T) \tag{50}$$

of $\omega_{\mathrm{u}}(t)$ and $\omega_{\mathrm{l}}(t)$. We make use of equations (38) and (42), and arrive at

$$\delta\phi_0 = \Phi(0) - 2\Phi\left(\frac{T}{2}\right) + \Phi(T) \tag{51}$$

describing the phase contribution arising from the position-independent potentials.

Next, we follow Step 2 of our analysis and identify according to figures 2 and 3(a) the functions

$$\mathbf{F}_{\mathrm{u}}(t) = \mathbf{F}_0 + \hbar\mathbf{k}\left[\delta(t) - \delta\left(t - \frac{T}{2}\right)\right] \tag{52}$$

for the upper and

$$\mathbf{F}_{\mathrm{l}}(t) = \mathbf{F}_0 + \hbar\mathbf{k}\left[\delta\left(t - \frac{T}{2}\right) - \delta(t - T)\right] \tag{53}$$

for the lower branch of the MZ interferometer having the difference

$$\delta\mathbf{F}(t) = \hbar\mathbf{k}\left[\delta(t) - 2\delta\left(t - \frac{T}{2}\right) + \delta(t - T)\right]. \tag{54}$$

Next, we check the closing conditions for this interferometer. The difference $\delta\mathbf{F}(t)$, equation (54), gives rise to the time-dependent vectors for the relative displacement in momentum

$$\delta\mathbf{p}(t) = \hbar\mathbf{k}\left[\Pi\left(t \,\middle|\, 0, \frac{T}{2}\right) - \Pi\left(t \,\middle|\, \frac{T}{2}, T\right)\right], \tag{55}$$

shown in figure 3(b), and in position

$$\delta\mathbf{r}(t) = \frac{\hbar\mathbf{k}}{m}\Lambda(t|0, T), \tag{56}$$

depicted in figure 3(c), according to equations (31) and (32). As evident from figures 3(b) and (c), and equations (55) and (56), we immediately prove that

[9] Here we use the notation $\nabla_z B_z = \frac{\partial B_z}{\partial z}(\mathbf{r} = 0)$ for the derivative of the z-component of the magnetic field $\mathbf{B} = \mathbf{B}(\mathbf{r})$ along the z-direction at the origin $\mathbf{r} = 0$. This derivative is assumed to be small compared to B_0, such that $L|\nabla_z B_z| \ll |B_0|$, where L is the total length of the interferometer. Moreover, we note that the form of the magnetic field given by equation (47) is an approximate one. Indeed, according to the Maxwell equation $\nabla \cdot \mathbf{B} = 0$, which is valid everywhere, a non-zero value of $\nabla_z B_z$ induces non-zero values of $\nabla_x B_x$ and $\nabla_y B_y$, such that $\nabla_x B_x + \nabla_y B_y = -\nabla_z B_z$, where B_x and B_y are the components of $\mathbf{B}$ along the x- and y-axis. However, in the limit of $L|\nabla_z B_z| \ll B_0$ the magnetic field $\mathbf{B}$ given by equation (47) is approximately directed along the z-axis.

$$\delta\mathbf{p}(t) = \delta\mathbf{r}(t) = 0 \tag{57}$$

for $t > T$, that is the MZ interferometer is closed. Thus, the interferometer contrast $C = 1$ and the interferometer phase

$$\delta\phi = \delta\phi_0 + \delta\phi_1 \tag{58}$$

is defined by equation (37), where $\delta\phi_0$ is given by equation (51).

In order to determine $\delta\phi_1$, we consider the average

$$\bar{\mathbf{F}}(t) = \mathbf{F}_0 + \frac{\hbar\mathbf{k}}{2}[\delta(t) - \delta(t-T)] \tag{59}$$

of $\mathbf{F}_u(t)$, equation (52), and $\mathbf{F}_l(t)$, equation (53). According to equation (39) and by using equation (56) we arrive at the second contribution to the interferometer phase

$$\delta\phi_1 = \frac{\mathbf{F}_0\mathbf{k}}{m}\int_0^T \mathrm{d}\tau\ \Lambda(\tau|0,\ T) + \frac{\mathbf{k}}{2}[\delta\mathbf{r}(0) - \delta\mathbf{r}(T)] = \frac{\mathbf{F}_0\mathbf{k}}{4m}T^2 \tag{60}$$

arising from the linear potentials, where we have used the fact that $\delta\mathbf{r}(0) = \delta\mathbf{r}(T) = 0$ and

$$\int_0^T \mathrm{d}\tau\ \Lambda(\tau|0,\ T) = \frac{T^2}{4} \tag{61}$$

being the area of a triangle with base T and height $T/2$ according to figure 3(c).

In the case of the gravitational field $\mathbf{F}_0 = m\mathbf{g}$ with the gravitational acceleration $\mathbf{g}$, we obtain for $T = 2T_1$ the familiar result $\mathbf{k}\mathbf{g}T_1^2$ [4, 5] for the phase $\delta\phi_1$, where T_1 is the time between the first and second laser pulse.

Moreover, the combination of a gravitational field and a magnetic field of constant gradient $\nabla_z B_z$ yields $\mathbf{F}_0 = m\mathbf{g} + \mu_z\nabla_z B_z\mathbf{e}_z$, and we obtain the result of [54].

4.2. T^3-interferometer

4.2.1. Description

We now move to the T^3-interferometer [77] having an interferometer phase scaling purely as T^3.

The key idea of this interferometer is to apply constant linear potentials with different magnitude to each of the two states $|1\rangle$ and $|2\rangle$. For this purpose we have suggested [77] to use two atomic states $|1\rangle$ and $|2\rangle$ having *different* mean values of the magnetic dipole moment $\boldsymbol{\mu}_{1,2}$ and expose them to the magnetic field $\mathbf{B}$, equation (47), with constant gradient $\nabla_z B_z$.

Thus, we obtain two different constant functions

$$\mathbf{F}_1 = \mathbf{F}_0 - \frac{1}{2}\Delta\mathbf{F} \tag{62}$$

and

$$\mathbf{F}_2 = \mathbf{F}_0 + \frac{1}{2}\Delta\mathbf{F} \tag{63}$$

assigned to the states $|1\rangle$ and $|2\rangle$, respectively, where

$$\mathbf{F}_0 = m\mathbf{g} + \frac{\mu_{1z} + \mu_{2z}}{2}\nabla_z B_z\mathbf{e}_z \tag{64}$$

and

$$\Delta\mathbf{F} = (\mu_{2z} - \mu_{1z})\nabla_z B_z\mathbf{e}_z. \tag{65}$$

The T^3-interferometer, as depicted in figure 4(a), consists of two beam-splitter pulses at the times $t_1 = 0$ and $t_4 = T$, while the two mirror pulses act at the times $t_2 = T/4$ and $t_3 = 3T/4$, where T is again the total interferometer time. The two mirror pulses are necessary to close the interferometer. Moreover, since co-propagating Raman pulses are used as beam-splitter and mirror pulses, we assume that there is no transfer of photon momentum to the atoms, that is we set $\mathbf{k} = 0$.

As shown in figure 4(b), the relative displacement in momentum $\delta\mathbf{p}(t)$ between the two arms of the interferometer is now piece-wise linear in t, whereas the relative displacement in position $\delta\mathbf{r}(t)$ presented in figure 4(c) is piece-wise quadratic in t, leading to a total interferometer phase scaling as T^3.

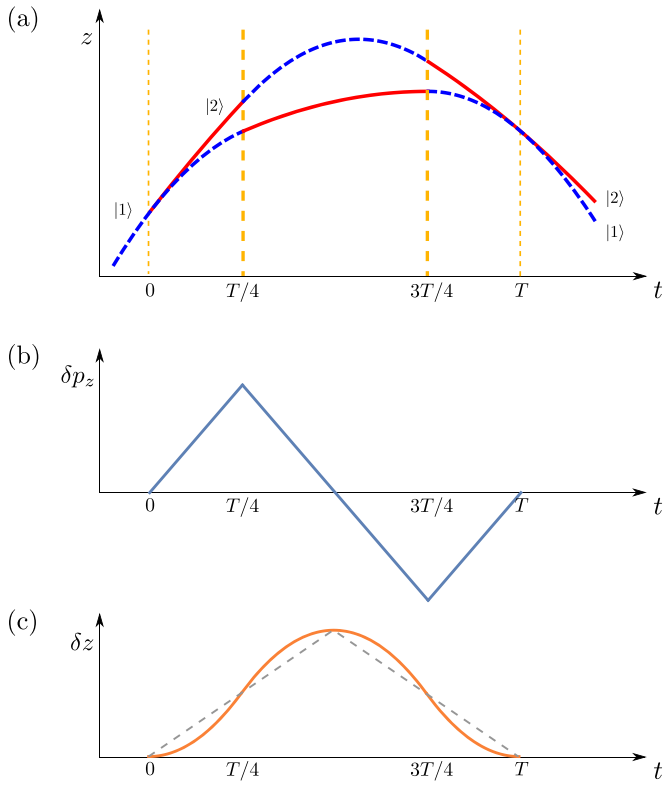

Figure 4. (a) Space-time diagram of the T^3-interferometer for an atom having two states $|1\rangle$ and $|2\rangle$ and interacting with two short laser $\pi/2$-pulses (at $t = 0$ and $t = T$) and two π-pulses (at $t = T/4$ and $t = 3T/4$), with T being the total interferometer time. We assume that during the light pulses there is no transfer of photon momentum to the atoms. Instead, the two states $|1\rangle$ (dashed blue line) and $|2\rangle$ (solid red line) are exposed to two different linear potentials. The z-component of the relative displacements in (b) momentum $\delta\mathbf{p}(t)$, equation (73), and (c) position $\delta\mathbf{r}(t)$, equation (74), for the T^3-interferometer as a function of the time t. The area enclosed by the two interferometer branches in the space-time diagram is the same as the one of the dashed triangle.

4.2.2. Analysis of the T^3-interferometer

According to Step 1 of our procedure (section 3.2) and to figures 2 and 4(a), we obtain the functions

$$\omega_{\mathrm{u}}(t) = -\Phi_{-}(0)\delta(t) + \Phi_{+}\left(\frac{T}{4}\right)\delta\left(t - \frac{T}{4}\right) - \Phi_{-}\left(\frac{3T}{4}\right)\delta\left(t - \frac{3T}{4}\right) + \Phi_{+}(T)\delta(t - T) \tag{66}$$

for the upper branch, together with

$$\omega_{\mathrm{l}}(t) = -\Phi_{-}\left(\frac{T}{4}\right)\delta\left(t - \frac{T}{4}\right) + \Phi_{+}\left(\frac{3T}{4}\right)\delta\left(t - \frac{3T}{4}\right) \tag{67}$$

for the lower branch of the T^3-interferometer, which determine the difference

$$\delta\omega(t) = -\Phi_{-}(0)\delta(t) + \left[\Phi_{+}\left(\frac{T}{4}\right) + \Phi_{-}\left(\frac{T}{4}\right)\right]\delta\left(t - \frac{T}{4}\right) - \left[\Phi_{-}\left(\frac{3T}{4}\right) + \Phi_{+}\left(\frac{3T}{4}\right)\right]\delta\left(t - \frac{3T}{4}\right) + \Phi_{+}(T)\delta(t - T). \tag{68}$$

By using equation (38), we obtain the first contribution to the interferometer phase

$$\delta\phi_0 = \Phi(0) - 2\Phi\left(\frac{T}{4}\right) + 2\Phi\left(\frac{3T}{4}\right) - \Phi(T) - \pi, \tag{69}$$

being determined by the position-independent potentials, where the last term $-\pi$ is a result of the *even* number of pulses used in this interferometer.

Next, we follow Step 2 of our procedure and obtain according to figures 2 and 4(a) the functions

$$\mathrm{F}_{\mathrm{u}}(t) = \mathrm{F}_2\Pi\left(t \,\middle|\, 0, \frac{T}{4}\right) + \mathrm{F}_1\Pi\left(t \,\middle|\, \frac{T}{4}, \frac{3T}{4}\right) + \mathrm{F}_2\Pi\left(t \,\middle|\, \frac{3T}{4}, T\right) \tag{70}$$

for the upper branch, together with

$$\mathbf{F}_{\mathrm{l}}(t) = \mathbf{F}_1\Pi\left(t \,\middle|\, 0, \frac{T}{4}\right) + \mathbf{F}_2\Pi\left(t \,\middle|\, \frac{T}{4}, \frac{3T}{4}\right) + \mathbf{F}_1\Pi\left(t \,\middle|\, \frac{3T}{4}, T\right) \tag{71}$$

for the lower branch of the T^3-interferometer, leading to the difference

$$\delta\mathbf{F}(t) = \Delta\mathbf{F}\left[\Pi\left(t \,\middle|\, 0, \frac{T}{4}\right) - \Pi\left(t \,\middle|\, \frac{T}{4}, \frac{3T}{4}\right) + \Pi\left(t \,\middle|\, \frac{3T}{4}, T\right)\right], \tag{72}$$

where we have used equations (62) and (63).

Next, we verify the closing conditions given by equations (35) and (36). Indeed, by applying equations (31) and (32) we obtain the relative displacement in momentum

$$\delta\mathbf{p}(t) = \Delta\mathbf{F}\left[\Lambda\left(t \,\middle|\, 0, \frac{T}{2}\right) - \Lambda\left(t \,\middle|\, \frac{T}{2}, T\right)\right] \tag{73}$$

shown in figure 4(b), and in position

$$\delta\mathbf{r}(t) = \frac{\Delta\mathbf{F}}{m}\Omega(t|0,\, T) \tag{74}$$

presented in figure 4(c). As evident from figures 4(b) and (c), and equations (73) and (74), we obtain

$$\delta\mathbf{p}(t) = \delta\mathbf{r}(t) = 0 \tag{75}$$

for $t > T$, that is the T^3-interferometer depicted in figure 4(a) is closed. Hence, its contrast $C = 1$ and its phase

$$\delta\phi = \delta\phi_0 + \delta\phi_1 \tag{76}$$

is defined by equation (37), where $\delta\phi_0$ is given by equation (69).

Now, we determine the phase contribution $\delta\phi_1$ and thus consider the average

$$\bar{\mathbf{F}}(t) = \mathbf{F}_0\Pi(t|0,\, T) \tag{77}$$

of $\mathbf{F}_{\mathrm{u}}(t)$, equation (70), and $\mathbf{F}_{\mathrm{l}}(t)$, equation (71), where we have used equations (62) and (63). According to equation (39) together with $\delta\mathbf{r}(t)$, equation (74), we obtain the phase contribution

$$\delta\phi_1 = \frac{\mathbf{F}_0\Delta\mathbf{F}}{\hbar m}\int_0^T \mathrm{d}\tau\ \Omega(\tau|0,\, T) = \frac{\mathbf{F}_0\Delta\mathbf{F}}{32\hbar m}T^3 \tag{78}$$

arising from the linear potentials, where we have used the fact that

$$\int_0^T \mathrm{d}\tau\ \Omega(\tau|0,\, T) = \frac{T^3}{32} \tag{79}$$

being the area of a triangle with base T and height $T^2/16$ according to the one presented in figure 4(c) by a gray dashed line.

These results entirely agree with the ones presented in [77] for $\mathbf{F}_0 = \frac{1}{2}m(a_1 + a_2)\mathbf{e}_z$, and $\Delta\mathbf{F} = m(a_2 - a_1)\mathbf{e}_z$, where $a_k\mathbf{e}_z\,(k = 1, 2)$ denotes the acceleration of the atom in the state $|k\rangle$ and $T = 4T_1$, with T_1 being the time between the first two laser pulses.

Moreover, it is interesting to note that the functions $\delta\mathbf{F}(t)$, equation (72), $\delta\mathbf{p}(t)$, equation (73), and $\delta\mathbf{r}(t)$, equation (74), are identical to the ones presented in the context of a Stern–Gerlach interferometer [93–95], where the time-dependence of these functions is not induced by applying mirror pulses, but by changing the direction of the magnetic field gradient at the time $T/4$ and $3T/4$. In this scheme [93–95] only the case $\mathbf{F}_0 = 0$ has been considered, and thus the cubic scaling of the interferometer phase did not occur in the analysis of the Stern–Gerlach interferometer.

4.3. CAB interferometer

4.3.1. Description

As pointed out in section 4.1, it is the fact that the relative displacement in position $\delta\mathbf{r}(t)$ is piece-wise linear in t that leads to a T^2 scaling in a standard MZ interferometer. Motivated by this argument, McDonald *et al* [76] suggested and implemented an interferometer in which the relative displacement $\delta\mathbf{r}(t)$ between the two branches is piece-wise proportional to $\alpha_0 t^2 + \beta_0 t$. Under these conditions, the interferometer phase scales as $\alpha_1 T^3 + \beta_1 T^2$ with α_i and $\beta_i\,(i = 0, 1)$ being constant. The interferometer scheme is similar to the MZ style interferometer, that is it employs the same pulse sequence with beam splitter pulses at $t_1 = 0$ and $t_3 = T$, separated by a mirror pulse at time $t_2 = T/2$. However, during the free evolution between the pulses, the state $|1\rangle$ is exposed to a *time-dependent* linear potential.

In this work [76], the beam splitter and mirror pulses are created by Bragg diffraction resulting in a momentum transfer $\pm n\hbar\mathbf{k}_1$, where n is the diffractive order and $\hbar\mathbf{k}_1$ is the momentum transfer for a first-order

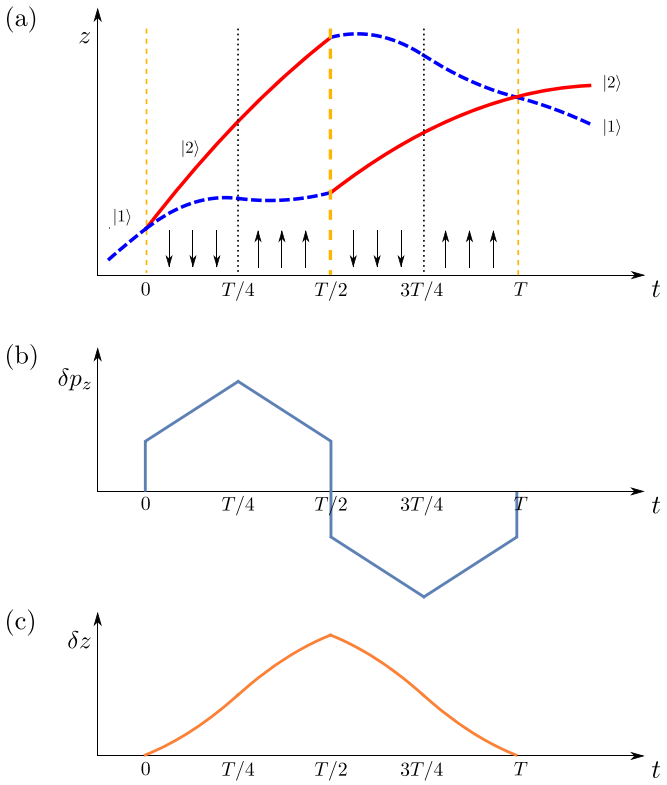

Figure 5. (a) Space-time diagram of the CAB interferometer for an atom having the states $|1\rangle$ and $|2\rangle$, and interacting with two short laser $\pi/2$-pulses (at $t = 0$ and $t = T$) and a π-pulse (at $t = T/2$). The state $|1\rangle$ (blue dashed line) is accelerated by a Bloch lattice, where the arrows indicate the direction of acceleration. However, the state $|2\rangle$ (solid red line) is exposed to a constant linear potential. The z-component of the relative displacements in (b) momentum $\delta\mathbf{p}(t)$, equation (88), and (c) position $\delta\mathbf{r}(t)$, equation (89), for the CAB interferometer as a function of the time t.

diffraction. After the first beam splitter pulse at $t = 0$, atoms in the momentum state labeled by $|1\rangle$ are loaded into a stationary optical lattice during the time T_r, accelerated via Bloch oscillations for a time T_b before being brought back to the initial acceleration during the time T_f. The loading time T_r and the deceleration time T_f are very short compared to the acceleration time T_b. The acceleration time T_b is hence approximately equal to the time $T/4$. In this way, the additional average acceleration

$$\Delta\mathbf{a} \equiv -\frac{2n_b\hbar\,\mathbf{k}_1}{mT_b} \tag{80}$$

imprinted by the Bloch lattice could be reinterpreted as the action of an effective linear potential during the time interval $(0, T/4)$, where n_b is the number of the Bloch oscillations imprinted during the time T_b.

Subsequently, as indicated by the arrows in figure 5(a), the direction of the acceleration $\Delta\mathbf{a}$ induced by the Bloch lattice is inverted and the sequence is repeated for the interval $(T/4, T/2)$. The lattice is moving sufficiently fast so that the atoms in the momentum state labeled by $|2\rangle$ experience only a time-averaged potential from the Bloch lattice which imparts no additional acceleration. In the following we will not consider the additional phase shift imprinted by this potential.

At time $t = T/2$ a Bragg π-pulse acts as mirror pulse and the same acceleration sequence is now applied to the other branch of the interferometer. A final $\pi/2$-pulse closes the interferometer.

As a result, atoms in the state $|2\rangle$ only experience a constant (background) linear potential described by

$$\mathbf{F}_2 = \mathbf{F}_0, \tag{81}$$

whereas the time-dependent linear potential experienced by atoms in the state $|1\rangle$ is determined by

$$\mathbf{F}_1(t) = \mathbf{F}_0 + \Delta\mathbf{F}\left[\Pi\left(t \,\middle|\, 0, \frac{T}{4}\right) - \Pi\left(t \,\middle|\, \frac{T}{4}, \frac{T}{2}\right) + \Pi\left(t \,\middle|\, \frac{T}{2}, \frac{3T}{4}\right) - \Pi\left(t \,\middle|\, \frac{3T}{4}, T\right)\right], \tag{82}$$

where

$$\Delta\mathbf{F} \equiv m\Delta\mathbf{a} = -\frac{2n_b\hbar\,\mathbf{k}_1}{T_b}. \tag{83}$$

Here we neglect the loading time T_r and the deceleration time T_f.

4.3.2. Analysis of the CAB interferometer

According to Step 1 of our procedure (section 3.2) and figures 2 and 5(a), we obtain the time-dependent functions $\omega_u(t)$, equation (48), for the upper path and $\omega_l(t)$, equation (49), for the lower path identical to the ones of the MZ interferometer discussed in section 4.1 as the same pulse sequence is used. Thus, we also arrive at the same phase contribution

$$\delta\phi_0 = \Phi(0) - 2\Phi\left(\frac{T}{2}\right) + \Phi(T) \tag{84}$$

for the CAB interferometer arising from the position-independent potentials.

Next, we follow Step 2 of our procedure and according to figures 2 and 5(a), we identify the functions

$$\mathbf{F}_u(t) = \hbar\mathbf{k}\left[\delta(t) - \delta\left(t - \frac{T}{2}\right)\right] + \mathbf{F}_2\Pi\left(t \,\middle|\, 0, \frac{T}{2}\right) + \mathbf{F}_1(t)\Pi\left(t \,\middle|\, \frac{T}{2}, T\right) \tag{85}$$

for the upper branch together with

$$\mathbf{F}_l(t) = \hbar\mathbf{k}\left[\delta\left(t - \frac{T}{2}\right) - \delta(t - T)\right] + \mathbf{F}_1(t)\Pi\left(t \,\middle|\, 0, \frac{T}{2}\right) + \mathbf{F}_2\Pi\left(t \,\middle|\, \frac{T}{2}, T\right) \tag{86}$$

for the lower branch of the CAB interferometer, where $\mathbf{F}_2$ and $\mathbf{F}_1(t)$ are given by equations (81) and (82), respectively. The difference of $\mathbf{F}_u(t)$ and $\mathbf{F}_l(t)$ yields[10]

$$\begin{aligned}\delta\mathbf{F}(t) = \hbar\mathbf{k}&\left[\delta(t) - 2\delta\left(t - \frac{T}{2}\right) + \delta(t - T)\right] \\ &- \Delta\mathbf{F}\left[\Pi\left(t \,\middle|\, 0, \frac{T}{4}\right) - \Pi\left(t \,\middle|\, \frac{T}{4}, \frac{3T}{4}\right) + \Pi\left(t \,\middle|\, \frac{3T}{4}, T\right)\right].\end{aligned} \tag{87}$$

We observe that $\delta\mathbf{F}(t)$ is a combination of the corresponding expressions for the MZ interferometer (section 4.1), equation (54), and the T^3-interferometer (section 4.2), equation (72).

In the next step, we check the closing conditions equations (35) and (36) for the CAB interferometer. According to equations (31) and (32), we obtain the time-dependent vectors for the relative displacement in momentum

$$\delta\mathbf{p}(t) = \hbar\mathbf{k}\left[\Pi\left(t \,\middle|\, 0, \frac{T}{2}\right) - \Pi\left(t \,\middle|\, \frac{T}{2}, T\right)\right] - \Delta\mathbf{F}\left[\Lambda\left(t \,\middle|\, 0, \frac{T}{2}\right) - \Lambda\left(t \,\middle|\, \frac{T}{2}, T\right)\right] \tag{88}$$

shown in figure 5(b) and in position

$$\delta\mathbf{r}(t) = \frac{\hbar\mathbf{k}}{m}\Lambda(t|0, T) - \frac{\Delta\mathbf{F}}{m}\Omega(t|0, T) \tag{89}$$

presented in figure 5(c).

As a result of equations (57) and (75), we immediately obtain

$$\delta\mathbf{p}(t) = \delta\mathbf{r}(t) = 0 \tag{90}$$

for $t > T$, resulting from the fact that both the MZ and the T^3-interferometer are closed. Hence the CAB interferometer is closed as well. Thus, its contrast $C = 1$ and its phase

$$\delta\phi = \delta\phi_0 + \delta\phi_1 \tag{91}$$

is defined by equation (37), where $\delta\phi_0$ is given by equation (84).

In order to determine the phase $\delta\phi_1$ we consider the average

$$\bar{\mathbf{F}}(t) = \frac{\hbar\,\mathbf{k}}{m}[\delta(t) - \delta(t - T)] + \frac{\mathbf{F}_1(t) + \mathbf{F}_2}{2}\Pi(t|0, T) \tag{92}$$

of $\mathbf{F}_u(t)$, equation (85), and $\mathbf{F}_l(t)$, equation (86). In contrast to the average functions $\bar{\mathbf{F}}$ for the MZ interferometer, equation (59), and the T^3-interferometer, equation (77), which are constant in the interval $0 < t < T$, due to the time-dependence of $\mathbf{F}_1(t)$, also the average $\bar{\mathbf{F}}(t)$ is now time-dependent during the interferometer sequence. However, as shown in appendix D, due to the symmetries of $\delta\mathbf{r}(t)$, equation (89), and $\bar{\mathbf{F}}(t)$, only the constant term $\mathbf{F}_0$ in $\mathbf{F}_2$, equation (81), and $\mathbf{F}_1(t)$, equation (82), will contribute to the phase shift $\delta\phi_1$ arising from the linear potentials. According to equation (39) we thus obtain the second contribution

[10] Here we use $\Pi^2(t|a, b) = \Pi(t|a, b)$, which is true for $t \neq a, b$. Moreover, $\Pi(a|a, b)$ and $\Pi(b|a, b)$ will not contribute to any integral independent of their exact value.

$$\delta\phi_1 = \frac{\mathbf{F}_0\mathbf{k}}{4m}T^2 - \frac{\mathbf{F}_0\Delta\mathbf{F}}{32\hbar m}T^3 \tag{93}$$

to equation (91), which is a combination of the corresponding phases for the MZ interferometer, equation (60), and the T^3-interferometer, equation (78).

In the case of $T = 2T_1, \mathbf{F}_0 = m\mathbf{a}, \mathbf{k} = 2n\mathbf{k}_1$, where T_1 denotes the time between the first two pulses and $\Delta\,\mathbf{F}$ is defined by equation (83) with $\tau_1 \equiv T_b/n_b$, this expression agrees with the one presented in [76].

It is remarkable, that even in this special case of a time-dependent average function $\bar{\mathbf{F}}(t)$, equation (92), the phase $\delta\phi_1$ is again proportional to the enclosed area between the two branches in the space-time diagram of the CAB interferometer.

5. Discussion

Section 3 represents one of the main features of this article—a methodology to analyze an atom interferometer consisting of two branches, assuming the atoms are exposed to linear potentials. More specifically, we formulated the rules for constructing two pairs of time-dependent functions $\{\mathbf{F}_u(t),\ \omega_u(t)\}$ and $\{\mathbf{F}_l(t),\ \omega_l(t)\}$ corresponding to the upper and lower branch of the interferometer, which depend on the pulse protocol and the (possible state-dependent) potentials the atoms move in. Once the potentials and the pulse sequence are specified, the functions $\delta\omega(t) = \omega_u(t) - \omega_l(t)$, $\delta\mathbf{F}(t) = \mathbf{F}_u(t) - \mathbf{F}_l(t)$, and $\bar{\mathbf{F}}(t) = \frac{1}{2}[\mathbf{F}_u(t) + \mathbf{F}_l(t)]$ are completely determined.

The function $\delta\mathbf{F}(t)$ defines the relative displacements in momentum $\delta\mathbf{p}(t)$ and position $\delta\mathbf{r}(t)$ of the two interferometer branches. Thus, in order to fulfill the closing conditions given by equations (31) and (32), an experimental control of the physical quantities determining $\delta\mathbf{F}(t)$ is necessary. Additionally, it is important to emphasize that the closing conditions are independent of the functions $\delta\omega(t)$ and $\bar{\mathbf{F}}(t)$, and hence the interferometer can be used to measure the physical quantities governing these functions. Under the condition that the interferometer is closed, its contrast equals unity and the functions $\delta\omega(t)$, $\bar{\mathbf{F}}(t)$, and $\delta\mathbf{r}(t)$ are used to determine the phase, equations (37), (38), and (39), of the interferometer, which is in this case independent of the initial state. The power of our methodology is shown in section 4.

5.1. Review of the three atom interferometers

In section 4, we presented the analysis of three interferometers: (a) the MZ interferometer, (b) the T^3-interferometer, and (c) the CAB interferometer. For all three cases, we derived the expression for $\delta\mathbf{F}(t)$ given by equations (54), (72) and (87), respectively, and used them to show that the interferometers are all closed. Closing occurs when both the relative displacement in momentum $\delta\mathbf{p}(t)$ and position $\delta\mathbf{r}(t)$ between the two branches of the interferometer vanishes for $t > T$, as demonstrated by equations (57), (75), and (90), respectively.

Of greater significance are the phases of these interferometers. In all three cases, the interferometer phase is written as the sum of two contributions: the phase $\delta\phi_0$ determined by the laser phases and the position-independent potentials, and the phase $\delta\phi_1$ due to the motion of the atoms in a linear potential.

We first focus on the expressions for the phase $\delta\phi_0$. For each type of interferometer this phase is given by equation (51), (69), and (84), accordingly, and is reproduced here again for convenience:

$$\delta\phi_0^{(\mathrm{MZ})} = \Phi(0) - 2\Phi\left(\frac{T}{2}\right) + \Phi(T), \tag{94}$$

$$\delta\phi_0^{(T^3)} = \Phi(0) - 2\Phi\left(\frac{T}{4}\right) + 2\Phi\left(\frac{3T}{4}\right) - \Phi(T) - \pi, \tag{95}$$

$$\delta\phi_0^{(\mathrm{CAB})} = \Phi(0) - 2\Phi\left(\frac{T}{2}\right) + \Phi(T), \tag{96}$$

where a superscript indicates the corresponding interferometer.

It is clear that the contribution for the CAB interferometer is identical to the one of the MZ interferometer, being a discrete second-order derivative of the function $\Phi(T)$, that is

$$\delta\phi_0^{(\mathrm{MZ})} \cong \frac{1}{4}\Phi''(0)\,T^2 \tag{97}$$

as $T \to 0$. However, for the T^3-interferometer we obtain instead a discrete third-order derivative of $\Phi(T)$, that is

$$\delta\phi_0^{(T^3)} \cong -\frac{1}{32}\Phi'''(0)\,T^3 - \pi \tag{98}$$

as $T \rightarrow 0$. It is interesting to note that the scaling with respect to T, and even the absolute value of the coefficients in equations (97) and (98) agree with the values of the integrals (61) and (79) determining the phase $\delta\phi_1$ for the MZ and the T^3-interferometer, respectively.

We now turn to a discussion of the contribution $\delta\phi_1$ of each interferometer, equations (60), (78), and (93), respectively, which we reproduce here for the ease of comparison:

$$\delta\phi_1^{(\mathrm{MZ})} = \frac{\mathbf{F}_0\mathbf{k}}{4m}T^2, \tag{99}$$

$$\delta\phi_1^{(T^3)} = \frac{\mathbf{F}_0\Delta\mathbf{F}}{32\hbar m}T^3, \tag{100}$$

$$\delta\phi_1^{(\mathrm{CAB})} = \frac{\mathbf{F}_0\mathbf{k}}{4m}T^2 - \frac{\mathbf{F}_0\Delta\mathbf{F}}{32\hbar m}T^3. \tag{101}$$

By comparing equations (99), (100) and (101), we immediately see that the CAB interferometer can be thought of as a hybrid between the standard MZ interferometer and the T^3-interferometer. The phase for the CAB interferometer is the sum of a contribution that scales as T^2, which is identical to the MZ T^2-phase, and a contribution that scales as T^3, which is identical to the T^3-term of the T^3-interferometer. However, it is important to bear in mind that the force difference $\Delta\mathbf{F}$ is caused by the application of a magnetic field gradient in the case of the T^3-interferometer, whereas it is generated by a Bloch lattice for the CAB interferometer.

5.2. Interpretation of the interferometer phase

Finally, we turn to an interpretation of the phase of the interferometer induced by the linear potentials. Examining equation (39), we observe that the contribution $\delta\phi_1$ is the integral of the product $\bar{\mathbf{F}}(t)\,\delta\mathbf{r}(t)$ for t between t_i and t_f. In the case of $\bar{\mathbf{F}}(t)$ being *time-independent* for $t_\mathrm{i} < t < t_\mathrm{f}$, as in the case of the MZ interferometer and the T^3-interferometer, this term is proportional to the *enclosed area* between the two branches in the space-time diagram of the interferometer displayed in figures 3(a) and 4 (a). However, even in the special case of the CAB interferometer where $\bar{\mathbf{F}}(t)$ is *time-dependent*, the phase contribution $\delta\phi_1$ is again proportional to the *enclosed area* of the interferometer in the space-time diagram, as discussed in section 4.3.2 and shown in figure 5(a).

The connection between the phase and the area enclosed by the interferometer in a space-time diagram was also analyzed within the semi-classical approach [67]. Our results are derived using only knowledge of the functions $\delta\mathbf{F}(t)$, $\delta\omega(t)$, and $\bar{\mathbf{F}}(t)$ and are completely consistent with the ones obtained in this reference.

Moreover, it is important to highlight that it is the *signed area*, which is relevant for the calculation of the interferometer phase. For example in the Butterfly geometry [86] the *signed area* vanishes, and the resulting interferometer phase becomes insensitive to $\bar{\mathbf{F}}$, assuming $\bar{\mathbf{F}}$ is *time-independent*. Hence, this device might be used to probe the influence of higher-order effects such as gravity gradients.

More generally, we can consider an interferometer having the pulse protocol $\frac{\pi}{2} - \pi - \ldots - \pi - \frac{\pi}{2}$, where the first and the last two pulses are each separated by the time T_1 and all other pulses have a separation time of $2T_1$. In the case that the force difference $\delta\mathbf{F}$ is only determined by the momentum transfer $\pm\hbar\mathbf{k}$ induced by the laser pulses, the dependence of the interferometer phase on $\bar{\mathbf{F}}$ is determined by the parity of the number of pulses. For an *odd* number of pulses the interferometer phase depends on $\bar{\mathbf{F}}$, whereas for an *even* number of pulses it is insensitive to a constant mean force $\bar{\mathbf{F}}$.

Intuitively, one might expect that the interferometer phase always scales with the enclosed area for a closed interferometer and arbitrary time-dependent linear potentials. However, since the closing conditions of the interferometer are only determined by $\delta\mathbf{F}(t)$, interferometers which are closed for a *time-independent* function $\bar{\mathbf{F}}$ will also be closed in the case that $\bar{\mathbf{F}}(t)$ is *time-dependent*. Therefore, the interferometer phase will in general not scale as the enclosed area. Nevertheless, it is interesting to ask the question which information about the time-dependent potentials determining $\bar{\mathbf{F}}(t)$ will be obtained by different interferometer schemes.

5.3. Limitations of our approach

In principle, we can consider within our approach additional effects such as finite pulse durations, gravity gradients, and rotations. However, in the case of finite pulse durations, both the pulse profile and the atomic motion during the atom–light interaction have to be taken into account, as discussed in [88, 89]. As a result, equations (10) and (12) for the beam-splitter and mirror operators would have to be modified: (i) the mirror operator, equation (12), will not have anti-diagonal form and instead contains also non-vanishing diagonal elements. This corresponds to the case that after each pulse new branches appear and it is impossible to describe the interferometer only based on two branches, as presented in our article. (ii) It is not any more possible to interpret the action of the pulses as being induced by effective linear potentials. Indeed, in addition to a phase shift and a displacement of the atomic center-of-mass wave packet in momentum as it is the case for a perfect

beam-splitter or mirror, the resulting complicated potentials also lead to a state-dependent distortion of the center-of-mass wave packet. The additional interferometer branches give rise to interferometer outputs depending on the initial state of the atomic center-of-mass motion as well as the parameters of the pulse. We emphasize that in most cases the resulting equations for an actual experimental setup can only be solved numerically.

Moreover, we point out that the representation-free approach presented in [86] valid for *state-independent* gravity gradients and rotations has already been generalized in [82] to *state-dependent* quadratic potentials. In the future it would be of interest to consider these effects within our simplified treatment.

6. Conclusion

In conclusion, we have considered atom interferometers exposed to time- and state-dependent linear potentials. We have studied the scaling of the output phase with T, the total interferometer time, for three types of atom interferometers—the MZ, the T^3-, and the CAB interferometer. To aid in the analysis, we have first developed a new formalism based simply on functions that were derived from the knowledge of the potentials in which the atoms move and the pulse sequence used for the interferometer. Our formalism leads directly to expressions for closing conditions in both momentum and position, which allow to immediately determine if an interferometer is closed. Additionally, the phase and contrast can also be obtained. We used this method to determine expressions for the phase of the three types of interferometers mentioned. In particular, we derived the well-known result that the phase of the MZ interferometer scales as T^2. Our results also confirm the ones presented in [77]. Here the phase for an interferometer using magnetically sensitive states with different mean values of the magnetic dipole moment and being exposed to an applied magnetic field gradient scales as T^3. Finally, we showed that the recently demonstrated CAB interferometer [76] is a hybrid between the standard MZ interferometer and the T^3-interferometer.

Acknowledgments

We acknowledge fruitful and interesting discussions on this topic with O Amit, R Folman, A Friedrich, S Kleinert, Y Margalit, A Roura, and C Ufrecht. This work is supported by the German-Israeli Project Cooperation DIP (project no. AR 924/1-1, DU 1086/2-1), as well as the German Space Agency (DLR) with funds provided by the Federal Ministry for Economic Affairs and Energy (BMWi) due to an enactment of the German Bundestag under Grants No. DLR 50WM1152-1157 (QUANTUS-IV) and the Centre for Quantum Engineering and Space-Time Research (QUEST). MAE is very grateful to the Center for Integrated Quantum Science and Technology (IQ^{ST}) for generous financial support. The research of the IQ^{ST} is financially supported by the Ministry of Science, Research and Arts Baden-Württemberg. WPS is most grateful to Texas A&M University for a Faculty Fellowship at the Hagler Institute for Advanced Study at the Texas A&M University as well as to the Texas A&M AgriLife Research for its support. FAN thanks the Office of the Secretary of Defense for a generous Laboratory University Collaboration Initiative (LUCI) grant.

Appendix A. Effective Hamiltonians for two interferometer branches

In this appendix we derive the effective Hamiltonian $\hat{H}_{\rm b}$ corresponding to the unitary operator $\hat{U}_{\rm b}$, equations (19)–(22), for the upper (b = u) and lower (b = l) branch of the interferometer, respectively.

First, we note that the unitary operator $\hat{E}_{kk}(t_{j+1},\, t_j)$ describing the free evolution of the atom in the state $|k\rangle$ from the time t_j to t_{j+1}, as defined by equations (6) and (7), is the time evolution operator of the Hamiltonian $\hat{H}_k$, equation (8), with $k = 1, 2$.

Second, following [80, 82], the unitary operator $\hat{L}_{\pm}(t_j)$ given by equation (11) can be identified as an evolution operator corresponding to the Hamiltonian

$$\hat{H}_{\pm}^{(L)} \equiv \mp\hbar\,[\mathbf{k}\hat{\mathbf{r}} + \Phi_{\mp}(t_j)]\,\delta(t - t_j), \tag{A.1}$$

where $\delta(t)$ denotes the Dirac delta function and

$$\Phi_{\mp}(t_j) \equiv \Phi(t_j) \mp \frac{\pi}{2}. \tag{A.2}$$

Now we are in the position to consider the time-ordered product of the unitary operators $\hat{L}_{\pm}$ and $\hat{E}_{kk}$, which determines the operators $\hat{U}_{\rm u}$ and $\hat{U}_{\rm l}$.

A.1. Effective Hamiltonians for an even number of pulses

In the case of an *even* number of pulses the operators $\hat{U}_{\rm u}$ and $\hat{U}_{\rm l}$ are given by equations (19) and (20). Using equations (7), (8), (11) and (A.1), we arrive at the Hamiltonians

$$\hat{H}_{\rm u}(t) \equiv \begin{cases} \hat{H}_{\rm l}, & t_{\rm i} \leqslant t \leqslant t_1^-, \\ \hat{H}_+^{(L)}, & t_1^- < t \leqslant t_1^+, \\ \hat{H}_2, & t_1^+ < t \leqslant t_2^-, \\ \hat{H}_-^{(L)}, & t_2^- < t \leqslant t_2^+, \\ \hat{H}_{\rm l}, & t_2^+ < t \leqslant t_3^-, \\ \vdots & \\ \hat{H}_+^{(L)}, & t_{n-1}^- < t \leqslant t_{n-1}^+, \\ \hat{H}_2, & t_{n-1}^+ < t \leqslant t_n^-, \\ \hat{H}_-^{(L)}, & t_n^- < t \leqslant t_n^+, \\ \hat{H}_{\rm l}, & t_n^+ < t \leqslant t_{\rm f}, \end{cases} \tag{A.3}$$

and

$$\hat{H}_{\rm l}(t) \equiv \begin{cases} \hat{H}_{\rm l}, & t_{\rm i} \leqslant t \leqslant t_2^-, \\ \hat{H}_+^{(L)}, & t_2^- < t \leqslant t_2^+, \\ \hat{H}_2, & t_2^+ < t \leqslant t_3^-, \\ \vdots & \\ \hat{H}_-^{(L)}, & t_{n-1}^- < t \leqslant t_{n-1}^+, \\ \hat{H}_{\rm l}, & t_{n-1}^+ < t \leqslant t_{\rm f}, \end{cases} \tag{A.4}$$

or

$$\hat{H}_{\rm b}(t) = \frac{\hat{\mathbf{p}}^2}{2m} - \mathbf{F}_{\rm b}(t)\hat{\mathbf{r}} + \hbar\omega_{\rm b}(t), \tag{A.5}$$

for (b = u, l) with the time-dependent functions

$$\mathbf{F}_{\rm u}(t) = \begin{cases} \mathbf{F}_{\rm l}, & t_{\rm i} \leqslant t \leqslant t_1^-, \\ +\hbar\mathbf{k}\delta(t-t_1), & t_1^- < t \leqslant t_1^+, \\ \mathbf{F}_2, & t_1^+ < t \leqslant t_2^-, \\ -\hbar\mathbf{k}\delta(t-t_2), & t_2^- < t \leqslant t_2^+, \\ \mathbf{F}_{\rm l}, & t_2^+ < t \leqslant t_3^-, \\ \vdots & \\ +\hbar\mathbf{k}\delta(t-t_{n-1}), & t_{n-1}^- < t \leqslant t_{n-1}^+, \\ \mathbf{F}_2, & t_{n-1}^+ < t \leqslant t_n^-, \\ -\hbar\mathbf{k}\delta(t-t_n), & t_n^- < t \leqslant t_n^+, \\ \mathbf{F}_{\rm l}, & t_n^+ < t \leqslant t_{\rm f}, \end{cases} \tag{A.6}$$

and

$$\omega_{\rm u}(t) = \begin{cases} 0, & t_{\rm i} \leqslant t \leqslant t_1^-, \\ -\Phi_-(t)\delta(t-t_1), & t_1^- < t \leqslant t_1^+, \\ 0, & t_1^+ < t \leqslant t_2^-, \\ +\Phi_+(t)\delta(t-t_2), & t_2^- < t \leqslant t_2^+, \\ \vdots & \\ -\Phi_-(t)\delta(t-t_{n-1}), & t_{n-1}^- < t \leqslant t_{n-1}^+, \\ 0, & t_{n-1}^+ < t \leqslant t_n^-, \\ +\Phi_+(t)\delta(t-t_n), & t_n^- < t \leqslant t_n^+, \\ 0, & t_n^+ < t \leqslant t_{\rm f}, \end{cases} \tag{A.7}$$

for the upper branch, and

$$\mathrm{F_l}(t) = \begin{cases} \mathrm{F_l}, & t_\mathrm{i} \leqslant t \leqslant t_2^-, \\ +\hbar\,\mathbf{k}\delta(t-t_2), & t_2^- < t \leqslant t_2^+, \\ \mathrm{F_2}, & t_2^+ < t \leqslant t_3^-, \\ \quad\vdots & \\ -\hbar\,\mathbf{k}\delta(t-t_{n-1}), & t_{n-1}^- < t \leqslant t_{n-1}^+, \\ \mathrm{F_l}, & t_{n-1}^+ < t \leqslant t_\mathrm{f}, \end{cases} \tag{A.8}$$

and

$$\omega_\mathrm{l}(t) = \begin{cases} 0, & t_\mathrm{i} \leqslant t \leqslant t_2^-, \\ -\Phi_-(t)\delta(t-t_2), & t_2^- < t \leqslant t_2^+, \\ \quad\vdots & \\ +\Phi_+(t)\delta(t-t_{n-1}), & t_{n-1}^- < t \leqslant t_{n-1}^+, \\ 0, & t_{n-1}^+ < t \leqslant t_\mathrm{f}, \end{cases} \tag{A.9}$$

for the lower branch of the interferometer. Here $t_j^\pm = t_j \pm t_\varepsilon$ with an infinitesimally small positive time t_ε and $j = 1, \ldots, n$.

A.2. Effective Hamiltonians for an odd number of pulses

In the case of an *odd* number of pulses we arrive at a slightly modified result, namely

$$\mathrm{F_u}(t) = \begin{cases} \mathrm{F_l}, & t_\mathrm{i} \leqslant t \leqslant t_1^-, \\ +\hbar\,\mathbf{k}\delta(t-t_1), & t_1^- < t \leqslant t_1^+, \\ \mathrm{F_2}, & t_1^+ < t \leqslant t_2^-, \\ -\hbar\,\mathbf{k}\delta(t-t_2), & t_2^- < t \leqslant t_2^+, \\ \mathrm{F_l}, & t_2^+ < t \leqslant t_3^-, \\ \quad\vdots & \\ -\hbar\,\mathbf{k}\delta(t-t_{n-1}), & t_{n-1}^- < t \leqslant t_{n-1}^+, \\ \mathrm{F_l}, & t_{n-1}^+ < t \leqslant t_\mathrm{f}, \end{cases} \tag{A.10}$$

and

$$\omega_\mathrm{u}(t) = \begin{cases} 0, & t_\mathrm{i} \leqslant t \leqslant t_1^-, \\ -\Phi_-(t)\delta(t-t_1), & t_1^- < t \leqslant t_1^+, \\ 0, & t_1^+ < t \leqslant t_2^-, \\ +\Phi_+(t)\delta(t-t_2), & t_2^- < t \leqslant t_2^+, \\ \quad\vdots & \\ +\Phi_+(t)\delta(t-t_{n-1}), & t_{n-1}^- < t \leqslant t_{n-1}^+, \\ 0, & t_{n-1}^+ < t \leqslant t_\mathrm{f}, \end{cases} \tag{A.11}$$

for the upper branch, as well as

$$\mathrm{F_l}(t) = \begin{cases} \mathrm{F_l}, & t_\mathrm{i} \leqslant t \leqslant t_2^-, \\ +\hbar\,\mathbf{k}\delta(t-t_2), & t_2^- < t \leqslant t_2^+, \\ \mathrm{F_2}, & t_2^+ < t \leqslant t_3^-, \\ \quad\vdots & \\ +\hbar\,\mathbf{k}\delta(t-t_{n-1}), & t_{n-1}^- < t \leqslant t_{n-1}^+, \\ \mathrm{F_2}, & t_{n-1}^+ < t \leqslant t_n^-, \\ -\hbar\,\mathbf{k}\delta(t-t_n), & t_n^- < t \leqslant t_n^+, \\ \mathrm{F_l}, & t_n^+ < t \leqslant t_\mathrm{f}, \end{cases} \tag{A.12}$$

and

$$\omega_{\rm l}(t) = \begin{cases} 0, & t_{\rm i} \leqslant t \leqslant t_2^-, \\ -\Phi_-(t)\delta(t-t_2), & t_2^- < t \leqslant t_2^+, \\ \vdots & \\ -\Phi_-(t)\delta(t-t_{n-1}), & t_{n-1}^- < t \leqslant t_{n-1}^+, \\ 0, & t_{n-1}^+ < t \leqslant t_n^-, \\ +\Phi_+(t)\delta(t-t_n), & t_n^- < t \leqslant t_n^+, \\ 0, & t_n^+ < t \leqslant t_{\rm f}, \end{cases} \tag{A.13}$$

for the lower branch of the interferometer.

As a result, the two effective Hamiltonians $\hat{H}_{\rm u}$ and $\hat{H}_{\rm l}$, equation (A.5), for the upper and lower branch of the interferometer describe the motion of a particle in a time-dependent linear potential with the time-dependent functions $\mathbf{F}_{\rm u}(t)$, $\mathbf{F}_{\rm l}(t)$, $\omega_{\rm u}(t)$, and $\omega_{\rm l}(t)$.

Appendix B. Propagation in a time-dependent linear potential

The motion of a particle of mass m in a linear potential is determined by the Hamiltonian

$$\hat{H}(t) = \frac{\hat{\mathbf{p}}^2}{2m} - \mathbf{F}(t)\hat{\mathbf{r}} + \hbar\omega(t), \tag{B.1}$$

with $\mathbf{F}(t)$ being a time-dependent vector and $\omega(t)$ a time-dependent scalar function. We represent the corresponding time evolution operator

$$\hat{U}(t,\, t_{\rm i}) = \exp\left[{\rm i}\phi(t)\right]\hat{D}\left[\mathbf{R}(t),\, \mathbf{P}(t)\right]\hat{U}_0(t,\, t_{\rm i}) \tag{B.2}$$

as a product [82, 83, 96] of the exponent of the phase factor $\phi(t)$, the displacement operator

$$\hat{D}[\mathbf{R},\, \mathbf{P}] = \exp\left[-\frac{\rm i}{\hbar}(\mathbf{R}\hat{\mathbf{p}} - \mathbf{P}\hat{\mathbf{r}})\right] \tag{B.3}$$

depending on the displacements in position $\mathbf{R}(t)$ and momentum $\mathbf{P}(t)$, and the evolution operator

$$\hat{U}_0(t,\, t_{\rm i}) = \exp\left[-\frac{\rm i}{\hbar}\frac{\hat{\mathbf{p}}^2}{2m}(t - t_{\rm i})\right] \tag{B.4}$$

for a free particle.

By following the approach presented in [82], we derive the equations for the time-dependent functions $\mathbf{R}(t)$, $\mathbf{P}(t)$ and $\phi(t)$ resulting from the Schrödinger equation

$${\rm i}\hbar\frac{\partial}{\partial t}\hat{U}(t,\, t_{\rm i}) = \hat{H}(t)\hat{U}(t,\, t_{\rm i}) \tag{B.5}$$

for the operator $\hat{U}(t,\, t_{\rm i})$ with the initial condition

$$\hat{U}(t_{\rm i},\, t_{\rm i}) = \mathbb{1}. \tag{B.6}$$

For this purpose, we insert equation (B.2) into the left hand side of equation (B.5)

$$\begin{aligned} {\rm i}\hbar\frac{\partial}{\partial t}\hat{U}(t,\, t_{\rm i}) = &\left\{-\hbar\dot{\phi}(t) + \left({\rm i}\hbar\frac{\partial}{\partial t}\hat{D}\left[\mathbf{R}(t),\, \mathbf{P}(t)\right]\right)\hat{D}^{\dagger}\left[\mathbf{R}(t),\, \mathbf{P}(t)\right]\right. \\ &\left. + \hat{D}\left[\mathbf{R}(t),\, \mathbf{P}(t)\right]\frac{\hat{\mathbf{p}}^2}{2m}\hat{D}^{\dagger}\left[\mathbf{R}(t),\, \mathbf{P}(t)\right]\right\} \\ &\times \exp\left[{\rm i}\phi(t)\right]\hat{D}\left[\mathbf{R}(t),\, \mathbf{P}(t)\right]\hat{U}_0(t,\, t_{\rm i}), \end{aligned} \tag{B.7}$$

where a dot denotes the derivative with respect to t and we have used the identity

$$\hat{D}^{\dagger}[\mathbf{R},\, \mathbf{P}]\hat{D}[\mathbf{R},\, \mathbf{P}] = \mathbb{1}. \tag{B.8}$$

The relation [97]

$$\begin{aligned} \frac{\rm d}{{\rm d}t}\exp\left[\hat{A}(t)\right] = &\left\{\frac{\rm d}{{\rm d}t}\hat{A}(t) + \frac{1}{2!}\left[\hat{A}(t),\, \frac{\rm d}{{\rm d}t}\hat{A}(t)\right]\right. \\ &\left. + \frac{1}{3!}\left[\hat{A}(t),\, \left[\hat{A}(t),\, \frac{\rm d}{{\rm d}t}\hat{A}(t)\right]\right] + \ldots\right\}\exp\left[\hat{A}(t)\right] \end{aligned} \tag{B.9}$$

for the derivative of the exponential operator $\exp[\hat{A}(t)]$ immediately gives rise to

$$\left(\mathrm{i}\hbar\frac{\partial}{\partial t}\hat{D}[\mathbf{R}(t),\,\mathbf{P}(t)]\right)\hat{D}^{\dagger}[\mathbf{R}(t),\,\mathbf{P}(t)] = \dot{\mathbf{R}}(t)\hat{\mathbf{p}} - \dot{\mathbf{P}}(t)\hat{\mathbf{r}} + \frac{1}{2}[\mathbf{R}(t)\dot{\mathbf{P}}(t) - \mathbf{P}(t)\dot{\mathbf{R}}(t)]. \tag{B.10}$$

Here we made use of the commutation relation

$$[\hat{r}_{\alpha},\,\hat{p}_{\beta}] = \mathrm{i}\hbar\delta_{\alpha\beta} \tag{B.11}$$

for the components $\hat{r}_{\alpha}$ of the position $\hat{\mathbf{r}}$ and $\hat{p}_{\beta}$ of the momentum $\hat{\mathbf{p}}$ operator ($\alpha, \beta = 1, 2, 3$), where $\delta_{\alpha\beta}$ denotes the Kronecker delta.

Next, we apply the Hadamard lemma [98]

$$e^{\hat{A}}\hat{B}e^{-\hat{A}} = \hat{B} + [\hat{A},\,\hat{B}] + \frac{1}{2!}[\hat{A},\,[\hat{A},\,\hat{B}]] + \ldots \tag{B.12}$$

for operators $\hat{A}$ and $\hat{B}$ together with the commutation relation equation (B.11), and obtain

$$\hat{D}[\mathbf{R}(t),\,\mathbf{P}(t)]\frac{\hat{\mathbf{p}}^2}{2m}\hat{D}^{\dagger}[\mathbf{R}(t),\,\mathbf{P}(t)] = \frac{1}{2m}[\hat{\mathbf{p}} - \mathbf{P}(t)]^2. \tag{B.13}$$

As a result, by using equations (B.5), (B.7), (B.10), and (B.13), we arrive at the relation

$$-\hbar\dot{\phi}(t) + \dot{\mathbf{R}}(t)\hat{\mathbf{p}} - \dot{\mathbf{P}}(t)\hat{\mathbf{r}} + \frac{1}{2}[\mathbf{R}(t)\dot{\mathbf{P}}(t) - \mathbf{P}(t)\dot{\mathbf{R}}(t)] - \frac{\mathbf{P}(t)}{m}\hat{\mathbf{p}} + \frac{\mathbf{P}^2(t)}{2m} = -\mathbf{F}(t)\hat{\mathbf{r}} + \hbar\omega(t) \tag{B.14}$$

for the unknown functions $\phi(t)$, $\mathbf{R}(t)$, and $\mathbf{P}(t)$.

By comparing the coefficients in front of the operators $\hat{\mathbf{p}}$ and $\hat{\mathbf{r}}$, as well as the remaining non-operator valued contribution, we obtain

$$\dot{\mathbf{P}}(t) = \mathbf{F}(t), \tag{B.15}$$

$$\dot{\mathbf{R}}(t) = \frac{\mathbf{P}(t)}{m}, \tag{B.16}$$

and

$$\dot{\phi}(t) = -\omega(t) + \frac{1}{2\hbar}[\mathbf{R}(t)\dot{\mathbf{P}}(t) - \mathbf{P}(t)\dot{\mathbf{R}}(t)] + \frac{\mathbf{P}^2(t)}{2\hbar m} = -\omega(t) + \frac{1}{2\hbar}\mathbf{F}(t)\mathbf{R}(t). \tag{B.17}$$

Note that equations (B.15) and (B.16) correspond to the classical equations of motion for a particle of mass m having the momentum $\mathbf{P}(t)$ and position $\mathbf{R}(t)$ and being exposed to the time-dependent force $\mathbf{F}(t)$.

Using the initial conditions

$$\mathbf{R}(t_{\mathrm{i}}) = \mathbf{P}(t_{\mathrm{i}}) = \phi(t_{\mathrm{i}}) = 0 \tag{B.18}$$

resulting from equations (B.2), (B.3), (B.4), and (B.6), we determine the functions

$$\mathbf{P}(t) = \int_{t_{\mathrm{i}}}^{t} \mathrm{d}\tau\ \mathbf{F}(\tau), \tag{B.19}$$

$$\mathbf{R}(t) = \frac{1}{m}\int_{t_{\mathrm{i}}}^{t} \mathrm{d}\tau_1 \int_{t_{\mathrm{i}}}^{\tau_1} \mathrm{d}\tau_2\ \mathbf{F}(\tau_2), \tag{B.20}$$

and

$$\phi(t) = \int_{t_{\mathrm{i}}}^{t} \mathrm{d}\tau\left[-\omega(\tau) + \frac{1}{2\hbar}\mathbf{F}(\tau)\mathbf{R}(\tau)\right]. \tag{B.21}$$

Appendix C. Interference of two branches

In section 2 we show that the contrast and phase of the interferometer are determined by the product $\hat{U}_{\mathrm{l}}^{\dagger}\hat{U}_{\mathrm{u}}$ of the evolution operator $\hat{U}_{\mathrm{b}}$, corresponding to the Hamiltonian

$$\hat{H}_{\mathrm{b}}(t) = \frac{\hat{\mathbf{p}}^2}{2m} - \mathbf{F}_{\mathrm{b}}(t)\hat{\mathbf{r}} + \hbar\omega_{\mathrm{b}}(t). \tag{C.1}$$

Here $\mathbf{F}_{\mathrm{b}}(t)$ and $\omega_{\mathrm{b}}(t)$ are the time-dependent functions for the upper ($\mathrm{b} = \mathrm{u}$) and lower ($\mathrm{b} = \mathrm{l}$) branch of the interferometer, as discussed in section 3. In order to evaluate $\hat{U}_{\mathrm{l}}^{\dagger}\hat{U}_{\mathrm{u}}$ we again follow the approach presented in [82].

By using equation (B.2) of appendix B, we obtain

$$\hat{U}_{\mathrm{l}}^{\dagger}(t,\,t_{\mathrm{i}})\,\hat{U}_{\mathrm{u}}(t,\,t_{\mathrm{i}}) = \exp\left\{\mathrm{i}[\phi_{\mathrm{u}}(t) - \phi_{\mathrm{l}}(t)]\right\}\hat{U}_{0}^{\dagger}(t,\,t_{\mathrm{i}})\hat{D}^{\dagger}[\mathbf{R}_{\mathrm{l}}(t),\,\mathbf{P}_{\mathrm{l}}(t)] \times \hat{D}[\mathbf{R}_{\mathrm{u}}(t),\,\mathbf{P}_{\mathrm{u}}(t)]\,\hat{U}_{0}(t,\,t_{\mathrm{i}}) \tag{C.2}$$

with the functions

$$\mathbf{P}_{\mathrm{u,l}}(t) = \int_{t_{\mathrm{i}}}^{t} \mathrm{d}\tau\; \mathbf{F}_{\mathrm{u,l}}(\tau), \tag{C.3}$$

$$\mathbf{R}_{\mathrm{u,l}}(t) = \frac{1}{m}\int_{t_{\mathrm{i}}}^{t} \mathrm{d}\tau_{1} \int_{t_{\mathrm{i}}}^{\tau_{1}} \mathrm{d}\tau_{2}\; \mathbf{F}_{\mathrm{u,l}}(\tau_{2}) \tag{C.4}$$

and

$$\phi_{\mathrm{u,l}}(t) = \int_{t_{\mathrm{i}}}^{t} \mathrm{d}\tau\left[-\omega_{\mathrm{u,l}}(\tau) + \frac{1}{2\hbar}\mathbf{F}_{\mathrm{u,l}}(\tau)\mathbf{R}_{\mathrm{u,l}}(\tau)\right] \tag{C.5}$$

given by equations (B.19)–(B.21) and corresponding to the upper and lower branch, respectively.

We first apply the commutation relation

$$\hat{D}[\mathbf{R},\,\mathbf{P}]\,\hat{U}_{0}(t,\,t_{\mathrm{i}}) = \hat{U}_{0}(t,\,t_{\mathrm{i}})\hat{D}\left[\mathbf{R} - \frac{\mathbf{P}}{m}(t - t_{\mathrm{i}}),\,\mathbf{P}\right] \tag{C.6}$$

and the identity

$$\hat{D}^{\dagger}[\mathbf{R},\,\mathbf{P}] = \hat{D}[-\mathbf{R},\,-\mathbf{P}] \tag{C.7}$$

in order to rewrite equation (C.2) as

$$\hat{U}_{\mathrm{l}}^{\dagger}(t,\,t_{\mathrm{i}})\,\hat{U}_{\mathrm{u}}(t,\,t_{\mathrm{i}}) = \exp\left\{\mathrm{i}[\phi_{\mathrm{u}}(t) - \phi_{\mathrm{l}}(t)]\right\}\hat{D}\left[-\mathbf{R}_{\mathrm{l}}(t) + \frac{\mathbf{P}_{\mathrm{l}}(t)}{m}(t - t_{\mathrm{i}}),\,-\mathbf{P}_{\mathrm{l}}(t)\right] \times \hat{D}\left[\mathbf{R}_{\mathrm{u}}(t) - \frac{\mathbf{P}_{\mathrm{u}}(t)}{m}(t - t_{\mathrm{i}}),\,\mathbf{P}_{\mathrm{u}}(t)\right], \tag{C.8}$$

where we have used the fact that

$$\hat{U}_{0}^{\dagger}(t,\,t_{\mathrm{i}})\,\hat{U}_{0}(t,\,t_{\mathrm{i}}) = \mathbb{1}. \tag{C.9}$$

In the next step, we use the identity

$$\hat{D}[\mathbf{R}_{1},\,\mathbf{P}_{1}]\hat{D}[\mathbf{R}_{2},\,\mathbf{P}_{2}] = \exp\left[\frac{\mathrm{i}}{2\hbar}(\mathbf{P}_{1}\mathbf{R}_{2} - \mathbf{P}_{2}\mathbf{R}_{1})\right]\hat{D}[\mathbf{R}_{1} + \mathbf{R}_{2},\,\mathbf{P}_{1} + \mathbf{P}_{2}] \tag{C.10}$$

for the displacement operator $\hat{D}[\mathbf{R},\,\mathbf{P}]$ and recast equation (C.8)

$$\hat{U}_{\mathrm{l}}^{\dagger}(t,\,t_{\mathrm{i}})\,\hat{U}_{\mathrm{u}}(t,\,t_{\mathrm{i}}) = \exp\left[\mathrm{i}\Delta\phi(t)\right]\hat{D}\left[\delta\mathbf{r}(t) - \frac{\delta\mathbf{p}(t)}{m}(t - t_{\mathrm{i}}),\,\delta\mathbf{p}(t)\right] \tag{C.11}$$

in terms of the relative displacements in momentum

$$\delta\mathbf{p}(t) = \mathbf{P}_{\mathrm{u}}(t) - \mathbf{P}_{\mathrm{l}}(t) = \int_{t_{\mathrm{i}}}^{t} \mathrm{d}\tau\; \delta\mathbf{F}(\tau) \tag{C.12}$$

and position

$$\delta\mathbf{r}(t) = \mathbf{R}_{\mathrm{u}}(t) - \mathbf{R}_{\mathrm{l}}(t) = \frac{1}{m}\int_{t_{\mathrm{i}}}^{t} \mathrm{d}\tau_{1} \int_{t_{\mathrm{i}}}^{\tau_{1}} \mathrm{d}\tau_{2}\; \delta\mathbf{F}(\tau_{2}) \tag{C.13}$$

with

$$\delta\mathbf{F}(t) \equiv \mathbf{F}_{\mathrm{u}}(t) - \mathbf{F}_{\mathrm{l}}(t), \tag{C.14}$$

as well as a phase factor

$$\Delta\phi(t) \equiv \phi_{\mathrm{u}}(t) - \phi_{\mathrm{l}}(t) + \frac{1}{2\hbar}[\mathbf{P}_{\mathrm{u}}(t)\mathbf{R}_{\mathrm{l}}(t) - \mathbf{P}_{\mathrm{l}}(t)\mathbf{R}_{\mathrm{u}}(t)]. \tag{C.15}$$

With equation (C.5) we arrive at

$$\phi_{\mathrm{u}}(t) - \phi_{\mathrm{l}}(t) = -\int_{t_{\mathrm{i}}}^{t} \mathrm{d}\tau\; \delta\omega(\tau) + \frac{1}{2\hbar}\int_{t_{\mathrm{i}}}^{t} \mathrm{d}\tau[\mathbf{F}_{\mathrm{u}}(\tau)\mathbf{R}_{\mathrm{u}}(\tau) - \mathbf{F}_{\mathrm{l}}(\tau)\mathbf{R}_{\mathrm{l}}(\tau)] \tag{C.16}$$

with

$$\delta\omega(t) \equiv \omega_{\mathrm{u}}(t) - \omega_{\mathrm{l}}(t). \tag{C.17}$$

By introducing

$$\bar{\mathbf{F}}(t) \equiv \frac{1}{2}[\mathbf{F}_{\mathrm{u}}(t) + \mathbf{F}_{\mathrm{l}}(t)] \tag{C.18}$$

and rewriting

$$\mathbf{F}_{\mathrm{u}}(\tau)\mathbf{R}_{\mathrm{u}}(\tau) - \mathbf{F}_{\mathrm{l}}(\tau)\mathbf{R}_{\mathrm{l}}(\tau) = 2\bar{\mathbf{F}}(\tau)\delta\mathbf{r}(\tau) + \mathbf{F}_{\mathrm{u}}(\tau)\mathbf{R}_{\mathrm{l}}(\tau) - \mathbf{F}_{\mathrm{l}}(\tau)\mathbf{R}_{\mathrm{u}}(\tau), \tag{C.19}$$

we recast equation (C.16) as

$$\phi_{\mathrm{u}}(t) - \phi_{\mathrm{l}}(t) = \int_{t_{\mathrm{i}}}^{t} \mathrm{d}\tau\left[-\delta\omega(\tau) + \frac{1}{\hbar}\bar{\mathbf{F}}(\tau)\delta\mathbf{r}(\tau)\right] + \frac{1}{2\hbar}\int_{t_{\mathrm{i}}}^{t} \mathrm{d}\tau[\mathbf{F}_{\mathrm{u}}(\tau)\mathbf{R}_{\mathrm{l}}(\tau) - \mathbf{F}_{\mathrm{l}}(\tau)\mathbf{R}_{\mathrm{u}}(\tau)]. \tag{C.20}$$

Now we show that the second integral in equation (C.20) equals the third term of the right-hand side of equation (C.15). Indeed, by using equations (B.15) and (B.16) we obtain

$$\begin{aligned}\frac{1}{2\hbar}\int_{t_{\mathrm{i}}}^{t} \mathrm{d}\tau[\mathbf{F}_{\mathrm{u}}(\tau)\mathbf{R}_{\mathrm{l}}(\tau) - \mathbf{F}_{\mathrm{l}}(\tau)\mathbf{R}_{\mathrm{u}}(\tau)] &= \frac{1}{2\hbar}\int_{t_{\mathrm{i}}}^{t} \mathrm{d}\tau[\dot{\mathbf{P}}_{\mathrm{u}}(\tau)\mathbf{R}_{\mathrm{l}}(\tau) - \dot{\mathbf{P}}_{\mathrm{l}}(\tau)\mathbf{R}_{\mathrm{u}}(\tau)] \\ &= \frac{1}{2\hbar}[\mathbf{P}_{\mathrm{u}}(t)\mathbf{R}_{\mathrm{l}}(t) - \mathbf{P}_{\mathrm{l}}(t)\mathbf{R}_{\mathrm{u}}(t)] - \frac{1}{2\hbar}\int_{t_{\mathrm{i}}}^{t} \mathrm{d}\tau[\mathbf{P}_{\mathrm{u}}(\tau)\dot{\mathbf{R}}_{\mathrm{l}}(\tau) - \mathbf{P}_{\mathrm{l}}(\tau)\dot{\mathbf{R}}_{\mathrm{u}}(\tau)] \\ &= \frac{1}{2\hbar}[\mathbf{P}_{\mathrm{u}}(t)\mathbf{R}_{\mathrm{l}}(t) - \mathbf{P}_{\mathrm{l}}(t)\mathbf{R}_{\mathrm{u}}(t)].\end{aligned} \tag{C.21}$$

As a result, equation (C.15) finally reads

$$\begin{aligned}\Delta\phi(t) = &\int_{t_{\mathrm{i}}}^{t} \mathrm{d}\tau\left[-\delta\omega(\tau) + \frac{1}{\hbar}\bar{\mathbf{F}}(\tau)\delta\mathbf{r}(\tau)\right] \\ &+ \frac{1}{2\hbar}\{\delta\mathbf{p}(t)[\mathbf{R}_{\mathrm{u}}(t) + \mathbf{R}_{\mathrm{l}}(t)] - \delta\mathbf{r}(t)[\mathbf{P}_{\mathrm{u}}(t) + \mathbf{P}_{\mathrm{l}}(t)]\}.\end{aligned} \tag{C.22}$$

C.1. Contrast and phase of an open interferometer

The contrast C and the phase $\delta\phi$ of an interferometer are determined by the matrix element

$$\langle\psi_{\mathrm{i}}|\hat{U}_{\mathrm{l}}^{\dagger}\hat{U}_{\mathrm{u}}|\psi_{\mathrm{i}}\rangle \equiv C\mathrm{e}^{\mathrm{i}\delta\phi} \tag{C.23}$$

of the operator product

$$\hat{U}_{\mathrm{l}}^{\dagger}\hat{U}_{\mathrm{u}} = \hat{U}_{\mathrm{l}}^{\dagger}(t_{\mathrm{f}}, t_{\mathrm{i}})\hat{U}_{\mathrm{u}}(t_{\mathrm{f}}, t_{\mathrm{i}}) \tag{C.24}$$

with respect to the initial state $|\psi_{\mathrm{i}}\rangle$, defined by equation (23), where t_{i} and t_{f} are the initial and final time of the interferometer, respectively.

By using equation (C.11), we obtain the contrast

$$C = \left|\langle\psi_{\mathrm{i}}|\ \hat{D}\left[\delta\mathbf{r}(t_{\mathrm{f}}) - \frac{\delta\mathbf{p}(t_{\mathrm{f}})}{m}(t_{\mathrm{f}} - t_{\mathrm{i}}),\ \delta\mathbf{p}(t_{\mathrm{f}})\right]|\psi_{\mathrm{i}}\rangle\right| \tag{C.25}$$

and the interferometer phase

$$\delta\phi = \Delta\phi(t_{\mathrm{f}}) + \phi_D, \tag{C.26}$$

where the wave packet independent contribution $\Delta\phi(t_{\mathrm{f}})$ is given by equation (C.22) and

$$\phi_D = \arg\left\{\langle\psi_{\mathrm{i}}|\ \hat{D}\left[\delta\mathbf{r}(t_{\mathrm{f}}) - \frac{\delta\mathbf{p}(t_{\mathrm{f}})}{m}(t_{\mathrm{f}} - t_{\mathrm{i}}),\ \delta\mathbf{p}(t_{\mathrm{f}})\right]|\psi_{\mathrm{i}}\rangle\right\} \tag{C.27}$$

describes the contribution depending on the initial state $|\psi_{\mathrm{i}}\rangle$. More details on open interferometers and wave packet dependent phases can be found in [81, 82].

C.2. Contrast and phase of a closed interferometer

In the case of a closed interferometer, that is

$$\delta\mathbf{p}(t_{\mathrm{f}}) = \delta\mathbf{r}(t_{\mathrm{f}}) = 0, \tag{C.28}$$

the displacement operator $\hat{D}$ in equations (C.25) and (C.27) is the identity implying $C = 1$. Moreover, the interferometer phase becomes independent of the initial state $|\psi_{\mathrm{i}}\rangle$ and is given by

$$\delta\phi = \Delta\phi(t_{\mathrm{f}}) = \int_{t_{\mathrm{i}}}^{t_{\mathrm{f}}} \mathrm{d}\tau\left[-\delta\omega(\tau) + \frac{1}{\hbar}\bar{\mathbf{F}}(\tau)\delta\mathbf{r}(\tau)\right], \tag{C.29}$$

where we have used equations (C.22), (C.27), and (C.28).

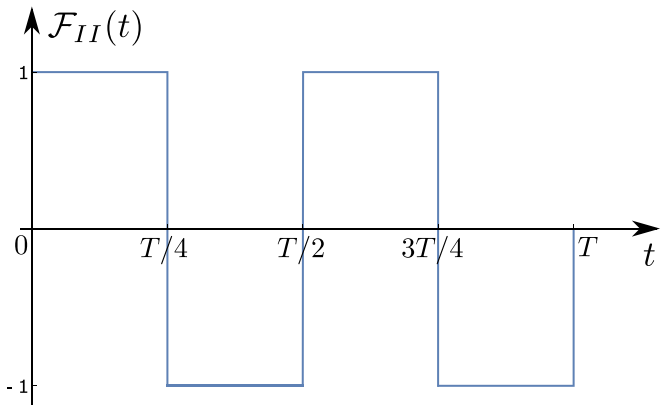

Figure D1. The function $\mathcal{F}_{\rm II}(t)$ defined by equation (D.3).

Appendix D. The phase $\delta\phi_1$ for the CAB interferometer

In this appendix we derive the second contribution $\delta\phi_1$ to equation (91) for the case of the CAB interferometer.

By using equations (81) and (82), we rewrite equation (92) (see footnote 8) as

$$\bar{\mathbf{F}}(t) = \mathbf{F}_0 + \frac{\hbar\mathbf{k}}{2}\mathcal{F}_{\rm I}(t) + \frac{\Delta\mathbf{F}}{2}\mathcal{F}_{\rm II}(t), \tag{D.1}$$

where we introduced the functions

$$\mathcal{F}_{\rm I}(t) \equiv \delta(t) - \delta(t - T) \tag{D.2}$$

and

$$\mathcal{F}_{\rm II}(t) \equiv \Pi\left(t \,\middle|\, 0, \frac{T}{4}\right) - \Pi\left(t \,\middle|\, \frac{T}{4}, \frac{T}{2}\right) + \Pi\left(t \,\middle|\, \frac{T}{2}, \frac{3T}{4}\right) - \Pi\left(t \,\middle|\, \frac{3T}{4}, T\right), \tag{D.3}$$

shown in figure D1.

As a result, according to equation (39) and by using equations (89) and (D.1), we obtain the second contribution to equation (91)

$$\delta\phi_1 = \frac{1}{\hbar}\int_{t_{\rm i}}^{t_{\rm f}} {\rm d}\tau\ \bar{\mathbf{F}}(\tau)\delta\mathbf{r}(\tau) \equiv \delta\varphi_0 + \delta\varphi_{\rm I} + \delta\varphi_{\rm II} \tag{D.4}$$

as a sum of three contributions determined by the corresponding terms in $\bar{\mathbf{F}}(t)$, equation (D.1).

The first contribution to the phase $\delta\phi_1$, equation (D.4), reads

$$\begin{aligned}\delta\varphi_0 &= \frac{1}{\hbar}\int_{t_{\rm i}}^{t_{\rm f}} {\rm d}\tau\ \mathbf{F}_0\delta\mathbf{r}(\tau)\\ &= \frac{\mathbf{F}_0\mathbf{k}}{m}\int_0^T {\rm d}\tau\ \Lambda(\tau|0,\ T) - \frac{\mathbf{F}_0\Delta\mathbf{F}}{\hbar m}\int_0^T {\rm d}\tau\ \Omega(\tau|0,\ T) = \frac{\mathbf{F}_0\mathbf{k}}{4m}T^2 - \frac{\mathbf{F}_0\Delta\mathbf{F}}{32\hbar m}T^3,\end{aligned} \tag{D.5}$$

where we have used equations (61) and (79).

The second contribution $\delta\varphi_{\rm I}$ to the phase $\delta\phi_1$ is governed by the function $\mathcal{F}_{\rm I}(\tau)$, equation (D.2), that is

$$\begin{aligned}\delta\varphi_{\rm I} &= \frac{\mathbf{k}}{2}\int_{t_{\rm i}}^{t_{\rm f}} {\rm d}\tau\ \mathcal{F}_{\rm I}(\tau)\delta\mathbf{r}(\tau)\\ &= \frac{\hbar\mathbf{k}^2}{2m}[\Lambda(T|0,\ T) - \Lambda(0|0,\ T)] - \frac{\mathbf{k}\Delta\mathbf{F}}{2m}[\Omega(T|0,\ T) - \Omega(0|0,\ T)] = 0\end{aligned} \tag{D.6}$$

with $\Lambda(0|0,\ T) = \Lambda(T|0,\ T) = 0$ and $\Omega(0|0,\ T) = \Omega(T|0,\ T) = 0$.

The third contribution $\delta\varphi_{\rm II}$ to the phase $\delta\phi_1$ is governed by the function $\mathcal{F}_{\rm II}(t)$, equation (D.3), that is

$$\delta\varphi_{\rm II} = \frac{\Delta\mathbf{F}}{2\hbar}\int_0^T {\rm d}\tau\ \mathcal{F}_{\rm II}(\tau)\delta\mathbf{r}(\tau) = \frac{\Delta\mathbf{F}}{2\hbar}\int_0^T {\rm d}\tau'\ \mathcal{F}_{\rm II}(T - \tau')\delta\mathbf{r}(T - \tau') = 0. \tag{D.7}$$

Here we have used the fact that

$$\delta\mathbf{r}(t) = \delta\mathbf{r}(T - t) \tag{D.8}$$

and

$$\mathcal{F}_{\rm II}(t) = -\mathcal{F}_{\rm II}(T - t). \tag{D.9}$$

Indeed, $\delta\mathbf{r}(t)$ is shown in figure 5(c) and consists of the functions $\Lambda(t|0,\ T)$, defined by equation (44), and $\Omega(t|0,\ T)$, defined by equation (45), which are even with respect to the point $t = T/2$. Moreover, as depicted in figure D1, the function $\mathcal{F}_{\rm II}(t)$, equation (D.3), is odd with respect to the point $t = T/2$.

Finally, according to equations (D.4)–(D.7), we obtain

$$\delta\phi_1 = \delta\varphi_0 = \frac{\mathbf{F}_0\mathbf{k}}{4m}T^2 - \frac{\mathbf{F}_0\Delta\mathbf{F}}{32\hbar m}T^3 \tag{D.10}$$

for the second contribution to equation (91).

References

[1] Keith D W, Ekstrom Ch R, Turchette Q A and Pritchard D E 1991 An interferometer for atoms *Phys. Rev. Lett.* **66** 2693–6
[2] Riehle F, Kisters Th, Witte A, Helmcke J and Bordé Ch J 1991 Optical Ramsey spectroscopy in a rotating frame: Sagnac effect in a matter-wave interferometer *Phys. Rev. Lett.* **67** 177–80
[3] Carnal O and Mlynek J 1991 Young's double-slit experiment with atoms: a simple atom interferometer *Phys. Rev. Lett.* **66** 2689–92
[4] Kasevich M and Chu S 1991 Atomic interferometry using stimulated Raman transitions *Phys. Rev. Lett.* **67** 181–4
[5] Kasevich M and Chu S 1992 Measurement of the gravitational acceleration of an atom with a light-pulse atom interferometer *Appl. Phys.* B **54** 321–32
[6] Ch R, Ekstrom J, Schmiedmayer M S, Chapman T D, Hammond and Pritchard D E 1995 Measurement of the electric polarizability of sodium with an atom interferometer *Phys. Rev.* A **51** 3883–8
[7] Miffre A, Jacquey M, Büchner M, Trénec G and Vigué J 2006 Measurement of the electric polarizability of lithium by atom interferometry *Phys. Rev.* A **73** 011603
[8] Gregoire M D, Hromada I, Holmgren W F, Trubko R and Cronin A D 2015 Measurements of the ground-state polarizabilities of Cs, Rb, and K using atom interferometry *Phys. Rev.* A **92** 052513
[9] Holmgren W F, Revelle M C, Lonij V P A and Cronin A D 2010 Absolute and ratio measurements of the polarizability of Na, K, and Rb with an atom interferometer *Phys. Rev.* A **81** 053607
[10] Degenhardt C, Stoehr H, Sterr U, Riehle F and Lisdat C 2004 Wavelength-dependent ac Stark shift of the $^1S_0^3P_1$ transition at 657 nm in Ca *Phys. Rev.* A **70** 023414
[11] Holmgren W F, Trubko R, Hromada I and Cronin A D 2012 Measurement of a wavelength of light for which the energy shift for an atom vanishes *Phys. Rev. Lett.* **109** 243004
[12] Trubko R, Gregoire M D, Holmgren W F and Cronin A D 2017 Potassium tune-out-wavelength measurement using atom interferometry and a multipass optical cavity *Phys. Rev.* A **95** 052507
[13] Weiss D S, Young B C and Chu S 1993 Precision measurement of the photon recoil of an atom using atomic interferometry *Phys. Rev. Lett.* **70** 2706–9
[14] Wicht A, Hensley J M, Sarajlic E and Chu S 2002 A preliminary measurement of the fine structure constant based on atom interferometry *Phys. Scr.* **2002** 82
[15] Cladé P, de Mirandes E, Cadoret M, Guellati-Khélifa S, Schwob C, Nez F, Julien L and Biraben F 2006 Precise measurement of $h/m_{\rm Rb}$ using Bloch oscillations in a vertical optical lattice: determination of the fine-structure constant *Phys. Rev.* A **74** 052109
[16] Cadoret M, de Mirandes E, Cladé P, Guellati-Khélifa S, Schwob C, Nez F, Julien L and Biraben F 2008 Combination of Bloch oscillations with a Ramsey-Bordé interferometer: new determination of the fine structure constant *Phys. Rev. Lett.* **101** 230801
[17] Bouchendira R, Cladé P, Guellati-Khélifa S, Nez F and Biraben F 2011 New determination of the fine structure constant and test of the quantum electrodynamics *Phys. Rev. Lett.* **106** 080801
[18] Barrett B, Carew A, Beattie S and Kumarakrishnan A 2013 Measuring the atomic recoil frequency using a modified grating-echo atom interferometer *Phys. Rev.* A **87** 033626
[19] Fixler J B, Foster G T, McGuirk J M and Kasevich M A 2007 Atom interferometer measurement of the Newtonian constant of gravity *Science* **315** 74–7
[20] Bertoldi A, Lamporesi G, Cacciapuoti L, de Angelis M, Fattori M, Petelski T, Peters A, Prevedelli M, Stuhler J and Tino G M 2006 Atom interferometry gravity-gradiometer for the determination of the Newtonian gravitational constant G *Eur. Phys. J.* D **40** 271–9
[21] Lamporesi G, Bertoldi A, Cacciapuoti L, Prevedelli M and Tino G M 2008 Determination of the Newtonian gravitational constant using atom interferometry *Phys. Rev. Lett.* **100** 050801
[22] Prevedelli M, Cacciapuoti L, Rosi G, Sorrentino F and Tino G M 2014 Measuring the Newtonian constant of gravitation G with an atomic interferometer *Phil. Trans. R. Soc.* A **372** 200
[23] Peters A, Chung K Y and Chu S 1999 Measurement of gravitational acceleration by dropping atoms *Nature* **400** 849
[24] Peters A, Chung K Y and Chu S 2001 High-precision gravity measurements using atom interferometry *Metrologia* **38** 25
[25] Zhou M-K, Hu Z-K, Duan X-C, Sun B-L, Chen L-L, Zhang Q-Z and Luo J 2012 Performance of a cold-atom gravimeter with an active vibration isolator *Phys. Rev.* A **86** 043630
[26] Malossi N, Bodart Q, Merlet S, Lévèque T, Landragin A and Pereira Dos Santos F 2010 Double diffraction in an atomic gravimeter *Phys. Rev.* A **81** 013617
[27] Lin Z, Zong-Yuan X, Wei Y, Biao T, Wen-Cui P, Yi-Bo W, Peng X, Jin W and Ming-Sheng Z 2011 Measurement of local gravity via a cold atom interferometer *Chin. Phys. Lett.* **28** 013701
[28] Schmidt M, Senger A, Hauth M, Freier C, Schkolnik V and Peters A 2011 A mobile high-precision absolute gravimeter based on atom interferometry *Gyrosc. Navig.* **2** 170
[29] Zhou L, Xiong Z Y, Yang W, Tang B, Peng W C, Hao K, Li R B, Liu M, Wang J and Zhan M S 2011 Development of an atom gravimeter and status of the 10 m atom interferometer for precision gravity measurement *Gen. Relativ. Gravit.* **43** 1931–42
[30] McGuinness H J, Rakholia A V and Biedermann G W 2012 High data-rate atom interferometer for measuring acceleration *Appl. Phys. Lett.* **100** 011106
[31] Merlet S, Bodart Q, Malossi N, Landragin A, Pereira Dos Santos F, Gitlein O and Timmen L 2010 Comparison between two mobile absolute gravimeters: optical versus atomic interferometers *Metrologia* **47** L9

[32] Debs J E, Altin P A, Barter T H, Döring D, Dennis G R, McDonald G, Anderson R P, Close J D and Robins N P 2011 Cold-atom gravimetry with a Bose–Einstein condensate *Phys. Rev.* A **84** 033610
[33] Charrière R, Cadoret M, Zahzam N, Bidel Y and Bresson A 2012 Local gravity measurement with the combination of atom interferometry and Bloch oscillations *Phys. Rev.* A **85** 013639
[34] Altin P A *et al* 2013 Precision atomic gravimeter based on Bragg diffraction *New J. Phys.* **15** 023009
[35] Bidel Y, Carraz O, Charrière R, Cadoret M, Zahzam N and Bresson A 2013 Compact cold atom gravimeter for field applications *Appl. Phys. Lett.* **102** 144107
[36] Hauth M, Freier C, Schkolnik V, Senger A, Schmidt M and Peters A 2013 First gravity measurements using the mobile atom interferometer gain *Appl. Phys.* B **113** 49–55
[37] Mok C, Barrett B, Carew A, Berthiaume R, Beattie S and Kumarakrishnan A 2013 Demonstration of improved sensitivity of echo interferometers to gravitational acceleration *Phys. Rev.* A **88** 023614
[38] Andia M, Jannin R, Nez F, Biraben F, Guellati-Khélifa S and Cladé P 2013 Compact atomic gravimeter based on a pulsed and accelerated optical lattice *Phys. Rev.* A **88** 031605
[39] Bonnin A, Zahzam N, Bidel Y and Bresson A 2013 Simultaneous dual-species matter-wave accelerometer *Phys. Rev.* A **88** 043615
[40] Hu Z-K, Sun B-L, Duan X-C, Zhou M-K, Chen L-L, Zhan S, Zhang Q-Z and Luo J 2013 Demonstration of an ultrahigh-sensitivity atom-interferometry absolute gravimeter *Phys. Rev.* A **88** 043610
[41] Biedermann G W, Wu X, Deslauriers L, Roy S, Mahadeswaraswamy C and Kasevich M A 2015 Testing gravity with cold-atom interferometers *Phys. Rev.* A **91** 033629
[42] Baryshev V N and Blinov I Y 2015 Application of atomic interferometers in gravimetry *Meas. Tech.* **57** 1333–7
[43] Barrett B, Bertoldi A and Bouyer P 2016 Inertial quantum sensors using light and matter *Phys. Scr.* **91** 053006
[44] Gustavson T L, Bouyer P and Kasevich M A 1997 Precision rotation measurements with an atom interferometer gyroscope *Phys. Rev. Lett.* **78** 2046–9
[45] Durfee D S, Shaham Y K and Kasevich M A 2006 Long-Term stability of an area-reversible atom-interferometer Sagnac gyroscope *Phys. Rev. Lett.* **97** 240801
[46] Dutta I, Savoie D, Fang B, Venon B, Garrido Alzar C L, Geiger R and Landragin A 2016 Continuous cold-atom inertial sensor with 1 nrad s^{-1} rotation stability *Phys. Rev. Lett.* **116** 183003
[47] Wu S, Su E and Prentiss M 2007 Demonstration of an area-enclosing guided-atom interferometer for rotation sensing *Phys. Rev. Lett.* **99** 173201
[48] McGuirk J M, Foster G T, Fixler J B, Snadden M J and Kasevich M A 2002 Sensitive absolute-gravity gradiometry using atom interferometry *Phys. Rev.* A **65** 033608
[49] Yu N, Kohel J M, Kellogg J R and Maleki L 2006 Development of an atom-interferometer gravity gradiometer for gravity measurement from space *Appl. Phys.* B **84** 647–52
[50] Bertoldi A, Lamporesi G, Cacciapuoti L, de Angelis M, Fattori M, Petelski T, Peters A, Prevedelli M, Stuhler J and Tino G M 2006 Atom interferometry gravity-gradiometer for the determination of the Newtonian gravitational constant G *Eur. Phys. J.* D **40** 271–9
[51] Sorrentino F, Lien Y-H, Rosi G, Cacciapuoti L, Prevedelli M and Tino G M 2010 Sensitive gravity-gradiometry with atom interferometry: progress towards an improved determination of the gravitational constant *New J. Phys.* **12** 095009
[52] Sorrentino F, Bodart Q, Cacciapuoti L, Lien Y-H, Prevedelli M, Rosi G, Salvi L and Tino G M 2014 Sensitivity limits of a Raman atom interferometer as a gravity gradiometer *Phys. Rev.* A **89** 023607
[53] D'Amico G, Borselli F, Cacciapuoti L, Prevedelli M, Rosi G, Sorrentino F and Tino G M 2016 Bragg interferometer for gravity gradient measurements *Phys. Rev.* A **93** 063628
[54] Davis J P and Narducci F A 2008 A proposal for a gradient magnetometer atom interferometer *J. Mod. Opt.* **55** 3173–85
[55] White G R, Lough J, Duncan D, Davis J P and Narducci F A 2009 Quantum optic techniques for diagnostics of a gradient magnetometer atom interferometer *J. Mod. Opt.* **56** 2013–21
[56] Zhou M-K, Hu Z-K, Duan X-C, Sun B-L, Zhao J-B and Luo J 2010 Precisely mapping the magnetic field gradient in vacuum with an atom interferometer *Phys. Rev.* A **82** 061602
[57] Barrett B, Chan I and Kumarakrishnan A 2011 Atom-interferometric techniques for measuring uniform magnetic field gradients and gravitational acceleration *Phys. Rev.* A **84** 063623
[58] Hu Q-Q, Freier C, Leykauf B, Schkolnik V, Yang J, Krutzik M and Peters A 2017 Mapping the absolute magnetic field and evaluating the quadratic Zeeman-effect-induced systematic error in an atom interferometer gravimeter *Phys. Rev.* A **96** 033414
[59] Canuel B *et al* 2006 Six-axis inertial sensor using cold-atom interferometry *Phys. Rev. Lett.* **97** 010402
[60] Müller T, Wendrich T, Gilowski M, Jentsch C, Rasel E M and Ertmer W 2007 Versatile compact atomic source for high-resolution dual atom interferometry *Phys. Rev.* A **76** 063611
[61] Dickerson S M, Hogan J M, Sugarbaker A, Johnson D M S and Kasevich M A 2013 Multiaxis inertial sensing with long-time point source atom interferometry *Phys. Rev. Lett.* **111** 083001
[62] de Angelis M, Bertoldi A, Cacciapuoti L, Giorgini A, Lamporesi G, Prevedelli M, Saccorotti G, Sorrentino F and Tino G M 2009 Precision gravimetry with atomic sensors *Meas. Sci. Technol.* **20** 022001
[63] Cronin A D, Schmiedmayer J and Pritchard D E 2009 Optics and interferometry with atoms and molecules *Rev. Mod. Phys.* **81** 1051–129
[64] Scully M O and Dowling J P 1993 Quantum-noise limits to matter-wave interferometry *Phys. Rev.* A **48** 3186–90
[65] Storey P and Cohen-Tannoudji C 1994 The Feynman path integral approach to atomic interferometry. A tutorial *J. Phys.* II **4** 1999–2027
[66] Barrett B, Geiger R, Dutta I, Meunier M, Canuel B, Gauguet A, Bouyer P and Landragin A 2014 The Sagnac effect: 20 years of development in matter-wave interferometry *C.R. Phys.* **15** 883
[67] McDonald G D and Kuhn C C N 2014 Space-time area in atom interferometry arXiv:1312.2713
[68] Berg P, Abend S, Tackmann G, Schubert Ch, Giese E, Schleich W P, Narducci F A, Ertmer W and Rasel E M 2015 Composite-light-pulse technique for high-precision atom interferometry *Phys. Rev. Lett.* **114** 063002
[69] Dunning A, Gregory R, Bateman J, Cooper N, Himsworth M, Jones J A and Freegarde T 2014 Composite pulses for interferometry in a thermal cold atom cloud *Phys. Rev.* A **90** 033608
[70] Lan S-Y, Kuan P-Ch, Estey B, Haslinger P and Müller H 2012 Influence of the Coriolis force in atom interferometry *Phys. Rev. Lett.* **108** 090402
[71] Chiow S W, Kovachy T, Chien H-C and Kasevich M A 2011 102$\hbar k$ large area atom interferometers *Phys. Rev. Lett.* **107** 130403
[72] Lévèque T, Gauguet A, Michaud F, Pereira Dos Santos F and Landragin A 2009 Enhancing the area of a Raman atom interferometer using a versatile double-diffraction technique *Phys. Rev. Lett.* **103** 080405

[73] Chiow S W, Herrmann S, Chu S and Müller H 2009 Noise-immune conjugate large-area atom interferometers *Phys. Rev. Lett.* **103** 050402
[74] McGuirk J M, Snadden M J and Kasevich M A 2000 Large area light-pulse atom interferometry *Phys. Rev. Lett.* **85** 4498–501
[75] Kotru K, Butts D L, Kinast J M and Stoner R E 2015 Large-area atom interferometry with frequency-swept Raman adiabatic passage *Phys. Rev. Lett.* **115** 103001
[76] McDonald G D, Kuhn C C N, Bennetts S, Debs J E, Hardman K S, Close J D and Robins N P 2014 A faster scaling in acceleration-sensitive atom interferometers *Europhys. Lett.* **105** 63001
[77] Zimmermann M, Efremov M A, Roura A, Schleich W P, DeSavage S A, Davis J P, Srinivasan A, Narducci F A, Werner S A and Rasel E M 2017 T^3-Interferometer for atoms *Appl. Phys.* B **123** 102
[78] Bongs K, Launay R and Kasevich M A 2006 High-order inertial phase shifts for time-domain atom interferometers *Appl. Phys.* B **84** 599–602
[79] Asenbaum P, Overstreet Ch, Kovachy T, Brown D D, Hogan J M and Kasevich M A 2017 Phase shift in an atom interferometer due to spacetime curvature across its wave function *Phys. Rev. Lett.* **118** 183602
[80] Schleich W P, Greenberger D M and Rasel E M 2013 A representation-free description of the Kasevich-Chu interferometer: a resolution of the redshift controversy *New J. Phys.* **15** 013007
[81] Roura A, Zeller W and Schleich W P 2014 Overcoming loss of contrast in atom interferometry due to gravity gradients *New J. Phys.* **16** 123012
[82] Zeller W 2016 The impact of wave-packet dynamics in long-time atom interferometry *PhD Thesis* Ulm University
[83] Bordé Ch J 1990 Propagation of laser beams and of atomic systems *Fundamental Systems in Quantum Optics* ed J Dalibard, J-M Raimond and J Zinn-Justin (Amsterdam: Elsevier) pp 287–380
[84] Bordé Ch J 2001 Theoretical tools for atom optics and interferometry *C. R. Acad. Sci.* **2** 509–30
[85] Antoine C and Bordé Ch J 2003 Quantum theory of atomic clocks and gravito-inertial sensors: an update *J. Opt.* B **5** S199–207
[86] Kleinert S, Kajari E, Roura A and Schleich W P 2015 Representation-free description of light-pulse atom interferometry including non-inertial effects *Phys. Rep.* **605** 50
[87] Schleich W P, Greenberger D M and Rasel E M 2013 Redshift controversy in atom interferometry: representation dependence of the origin of phase shift *Phys. Rev. Lett.* **110** 010401
[88] Audretsch J and Marzlin K-P 1994 Atom interferometry with arbitrary laser configurations: exact phase shift for potentials including inertia and gravitation *J. Phys.* II **4** 2073–87
[89] Lämmerzahl C and Bordé Ch J 1995 Rabi oscillations in gravitational fields: exact solution *Phys. Lett.* A **203** 67
[90] Giese E Mechanisms of matter-wave diffraction and their application to interferometers *Fortschr. Phys.* **63** 337–410
[91] Moler K, Weiss D S, Kasevich M and Chu S 1992 Theoretical analysis of velocity-selective Raman transitions *Phys. Rev.* A **45** 342–8
[92] Giese E, Zeller W, Kleinert S, Meister M, Tamma V, Roura A and Schleich W P 2014 The interface of gravity and quantum mechanics illuminated by Wigner phase space *Proceedings of the International School of Physics Enrico Fermi Course* vol 188, ed G M Tino and M A Kasevich (Amsterdam: IOS Press) pp 171–236
[93] Englert B-G, Schwinger J and Scully M O 1988 Is spin coherence like Humpty-Dumpty? I. Simplified treatment *Found. Phys.* **18** 1045–56
[94] Schwinger J, Scully M O and Englert B-G 1988 Is spin coherence like Humpty-Dumpty? II. General theory *Z. Phys.* D **10** 135–44
[95] Scully M O, Englert B-G and Schwinger J 1989 Spin coherence and Humpty-Dumpty: III. The effects of observation *Phys. Rev.* A **40** 1775–84
[96] Hogan J M, Johnson D M S, Kasevich M A, Arimondo E, Ertmer W, Schleich W P and Rasel E M 2009 Light-pulse atom interferometry *Proceedings of the International School of Physics Enrico Fermi* vol 168, ed E Arimondo *et al* (Amsterdam: IOS Press) pp 411–47
[97] Hall B C 2015 *Lie Groups, Lie Algebras, and Representations: An Elementary Introduction* (Berlin: Springer)
[98] Wilcox R M 1967 Exponential operators and parameter differentiation in quantum physics *J. Math. Phys.* **8** 962–82